Understanding The Dynamics Of Vapor Intrusion Processes

Brown University

Jonathan G. V. Ström

Spring 2020

Contents

Chapter 1

Introduction

1.1 Indoor Air Quality & Vapor Intrusion

Concerns about air quality are as old as civilization itself, ranging from beliefs that disease is caused by bad air - a *miasma*, to more recent concerns about exposure to combustion particulates, radon gas, or other air-borne pollutants. Since industrialization the number of potential hazardous pollutants has increased significantly, followed by increased concerns about air quality. At the same time, people now spend more time indoors now than ever before, with Americans spending up to 90% of their waking time indoors[**klepeis˙national˙2001**]. This change in human habitation has put a special emphasis on indoor air quality.

Some early scientific inquiries into indoor air quality focused on pollutant sources that were generated in the home, e.g. by heating and cooking systems, and these types of pollutants are still relevant today, but of particular concern in developing countries[**craig˙d.˙hollowell˙combustion-generated˙1976**, **world˙health˙organisation˙who**
Many buildings materials can also cause indoor air quality issues, with exposure to asbestos fibers being perhaps one of the more famous examples of this. Mold is another common indoor quality concern[**world˙health˙organisation˙who˙2009**].

In the 1970s, to address the growing public health concerns, research began into the potential exposure to radioactive radon gas in buildings. Radon gas, which is generated by the decay of naturally occurring uranium in soils and rocks, was found to be able to enter overlying building and expose the inhabitants. This phenomena came to the public attention in the mid 1980s, after a Pennsylvanian nuclear power plant worker set off radioactivity sensors at the plant, the cause of which was the high concentration of radon gas in the workers home[**noauthor˙health˙nodate**]. Exposure to radon gas can significantly increase the risk of developing lung cancer, and is to this day the second leading cause of lung cancer in many countries[**gaskin˙janet˙global˙nodate**
With the discovery of radon intrusion into buildings, it did not take long for the same concerns to be extended to the entry of anthropogenic contaminant vapors - vapor intrusion (VI).

Vapor intrusion is the migration of contaminant vapors from a contaminant source, often contaminated groundwater, into the overlying buildings. These vapors evaporate from the contaminated groundwater and enter through cracks in the building foundation, gaps between walls and floors, sump pits, or other openings[**u.s.˙environmental˙p**
In these aspects, VI is more or less similar to radon intrusion, and thus much of the early VI research was heavily influenced by the work done by radon intrusion

researchers. This is largely true to this day, but vapor intrusion differs in some non-trivial ways, that make it an unique issue. Many of these differences stem from the properties of the contaminants themselves, and from the fact that many of the VI contaminants that we concern ourselves with, mainly volatile organic compounds (VOCs) and chlorinated solvents, are of anthropogenic origins.

One difference is that radon is unstable, and has a half-life of around 3.8 days (at least Rn^{222}, the only naturally occurring isotope of radon), and it follows that radon accumulation will be naturally mitigated, which is not the case with other contaminants[**schumacher˙fluctuation˙2012**]. The closest analogy is that certain VOCs of VI concern are able to be biodegraded by bacteria in the soil, but this effect can vary significantly as this process is oxygen limited[**u.s.˙environmental˙protection˙agency˙oswer˙
abreu˙simulating˙2006**].

A more significant difference is the anthropogenic origin of VI contaminants. In VI, we often are concerned with a contaminated groundwater source underneath the afflicted building, and the source of the groundwater contamination typically originates from some contaminant spill at one or more sites in the surrounding area. Thus, a large number of buildings may be impacted by VI via a single contaminant source. The origins of such spills are numerous, but any activities that employ the contaminants of VI concern are possible culprits[**u.s.˙environmental˙protection˙agency˙oswer˙2015**]
In the United States (US), the Environmental Protection Agency (EPA) maintains a list of polluted sites throughout the country, so called Superfund sites, and as of 2020 there are 1335 recorded sites, many of which contain the contaminants of concern[**us˙epa˙current˙2015**, **u.s.˙environmental˙protection˙agency˙oswer˙2015**]. Additionally, many of the contaminants of concern do not readily degrade, and legacy contamination is an issue[**u.s.˙environmental˙protection˙agency˙oswer˙2015**].

In VI, some common contaminants of concern are chlorinated solvents such as trichloroethylene (TCE), tetrachloroethylene (PCE), or chloroform. Various other organic compounds such as benzene, or other petroleum products are also of concern. Out of the various VI contaminants, TCE has emerged as of perhaps particular concern, mostly due to its associated cancer risk. TCE is an excellent degreaser and has seen extensive use as such, and has been commonly used by dry cleaners, the military, auto repair shops etc[**u.s.˙environmental˙protection˙agency˙oswer˙2015**]. Despite concerns about its health effects, its use remains legal.

Considering the widespread existence of potential VI sites and the associated health concerns, an industry for finding these sites and either remediating or mitigating them has emerged. However, as we will see in this work, this has not been easy, and while VI has been studied for decades, many questions and challenges remain, in particular with regards to the great spatial and temporal variability that exist both within and between VI sites[**u.s.˙environmental˙protection˙agency˙oswer˙2015**].

1.2 Issues In Vapor Intrusion Investigations

Determining if vapor intrusion occurs at a building is often difficult. One might be tempted to believe that collecting an indoor air sample inside the building would be sufficient, i.e. that if the vapor contaminant concentrations is over some threshold in the house, proves that IV occurs, and the absence of contaminant vapors is proof that no VI occurs. However, this approach is too simplistic and may yield false positives.

Many common consumer products contain the same contaminants that are of concern in VI, and the presence in the home of e.g. a petroleum containing gasoline tank may be the culprit. Not all indoor contaminant sources are so obvious though, and many contaminants may be inadvertently introduced, such as by bringing home newly dry-cleaned clothing (a common source of PCE). Great care is taken to eliminate such indoor sources during formal VI investigations, but can be challenging.

A compounding issue related to this is that many of the contaminants can sorb onto/into various materials and subsequently desorb for significant periods of time, potentially extending the influence of indoor source beyond their removal[**meininghaus˙diffusion meininghaus˙diffusion˙2002**]. This a phenomena, among other related issues with sorption, we will discuss in Chapter (TBD).

Since indoor air sampling may not alone prove that VI occurs, investigations usually involve further steps. One is to collect air samples right below the foundation of the building, and if contaminant vapors are found there, as well as in the indoor air, that is more compelling evidence that VI occurs. However, as work by **holton˙creation˙2018**[**holton˙creation˙2018**] has shown, contaminant vapors in the indoor environment may migrate from inside the building to the subslab, creating a contaminant cloud in soil beneath the building that may persist for significant periods of time.

Collecting samples from the contaminant source, such as the groundwater underneath a building, to determine the presence of contaminants can be used as potential evidence of VI. However, even identifying such a potential source is not enough evidence of VI, as the presence of a contaminant source does not mean that the contaminant vapor actually enters the overlying building. **folkes˙observed˙2009**[**folkes˙observed˙2009**] conducted a decade long study of VI sites in Redfield, Colorado, and a 19 month long study in New York showed that many of the sites, even though they were above a contaminated groundwater source, were not impacted by VI.

Often investigators take samples from different locations, those already discussed as well as soil-gas samples, and compare the relative decrease in contaminant vapor concentration from the source to the indoor to establish what is termed a "completed pathway". This decrease is called *attenuation* and is quantitively represented in concentration from one point to the next as an *attenuation factor*. For example, the indoor contaminant concentration is divided by the contaminant concentration at the soil-gas groundwater interface. α is commonly used in this work we will often use a subscript to denote attenuation from one measurement point to another. In the case of groundwater attenuation for instance, one would divide the indoor contaminant concentration by the groundwater contaminant vapor concentration (that is when the contaminant concentration is in equilibrium with air, e.g. Henry's Law).

$$\alpha_{\mathrm{gw}} = \frac{c_{\mathrm{in}}}{c_{\mathrm{gw}} K_H} \tag{1.1}$$

Where α_{gw} is the attenuation from groundwater; c_{in} [$\mathrm{mol\,m^{-3}}$] is the indoor contaminant concentration; c_{gw} [$\mathrm{mol\,m^{-3}}$] is the groundwater *liquid phase* contaminant concentration; and K_H is the dimensionless Henry's Law constant.

Over time, the U.S. Environmental Protection Agency (EPA) has compiled data on attenuation factors relative to different source depths and types. Using these data, standards as to which attenuation factors are expected have been established to help guide investigators and regulator determine the VI risk. This is helpful, but

often we are faced with VI sites that render these sort of standards difficult to use.

Heterogeneity in soil, nonhomogeneous contaminant source concentration, as well as differences in the nature of the source (e.g. a contaminant spill in the soil itself vs. a leaky underground chemical tank), can all contribute to significant spatial variability in contaminant concentration at a site. A good example of this is seen in a study by **luo˙spatial˙2009**[**luo˙spatial˙2009**] where contaminant concentration beneath a building foundation varied from 200 to less than 0.01 mg/L. **bekele˙influence˙2014**[**bekele˙influence˙2014**] also found that TCE soil-gas concentration could vary by an order of magnitude underneath the foundation of another site.

Likewise, not all indoor environments are perfectly mixed and indoor contaminant concentration can vary significantly between different rooms or compartments in a building. This was observed at a site in Boston, Massachusetts by **pennell˙sewer˙2013**[**pennell˙sew** who found that the indoor contaminant concentration was significantly higher in the upstairs bathroom than in the basement, where one typically would expect higher concentrations.

The work by **pennell˙sewer˙2013**[**pennell˙sewer˙2013**] further revealed that VI could occur through sewers and enter the building through broken plumbing fixtures, which requires considering another level of complexity in VI - associated with the existence of preferential pathways. A preferential pathway is a term used describe something permitting enhanced contaminant vapor transport to near or into a building, in contrast with the more "traditional" view that contaminant transport occurs through soil. **mchugh˙evidence˙2017**[**mchugh˙evidence˙2017**] studied a VI impacted building in Indianapolis, Indiana, and found that the sewer system there acted as a preferential pathway bringing contaminants into the house (in addition to the soil pathway from the contaminated groundwater). There contaminated groundwater infiltrated into the sewer system a few blocks away from the site.

Similarly, **guo˙identification˙2015**[**guo˙identification˙2015**] studied a site in Layton, Utah, that was found to be impacted by a sewer connected land drain that allowed contaminant vapors to be transported to the near-slab region beneath a house (and close to a visible breach in the foundation). The results of this study and the role of the preferential pathway is a significant focus of this work and will be discussed in more detail in Chapter (TBD).

holton˙temporal˙2013[**holton˙temporal˙2013**] (same group as **guo˙identification˙2015**) demonstrated the very significant temporal variability in indoor contaminant concentrations that exist at some sites, where they found close to four orders of magnitude in variability during the multi-year study period. **hosangadi˙high-frequency˙2017**[**hosangadi˙high-f** studied another site in San Diego, California, that likewise showed orders of magnitude temporal variability, albeit on a shorter time scale. Likewise, the aforementioned site in Indianapolis exhibited significant temporal variability[**schumacher˙fluctuation˙2012**].

This temporal variability often has a seasonal component, and the highest indoor contaminant concentrations are usually found during the colder months of the year[**schumacher˙fluctuation˙2012**, **holton˙temporal˙2013**], although there are cases when the opposite is true. **steck˙indoor˙2004**[**steck˙indoor˙2004**] shows this at a radon impacted building in Minnesota, where the highest radon levels where observed during summer. Some authors such as **bekele˙influence˙2014**[**bekele˙influence˙2014**] suggest that it may be necessary to collect samples at intervals across a full year, to account for all seasonal effects, to avoid mischaracterization of VI.

The complexity and nuances of VI has made it necessary for a multiple lines-of-evidence (MLE) approach to be taken when determining if a building is impacted by VI[**u.s.˙environmental˙protection˙agency˙oswer˙2015**, **pennell˙field˙2016**]. However, the complexities associated with this approach has prompted the development of new methodologies and techniques that can reduce the uncertainty and complexity associated with conducting VI site investigations.

1.3 Innovations In Vapor Intrusion Investigations

In an attempt to reduce the uncertainty in determining human exposure due to vapor intrusion caused by the significant spatial and temporal variability in VI, a number of new investigatory techniques and methods have been proposed, but in general their efficacy is yet to be fully established[**mchugh˙recent˙2017**]. This work won't deal with all of these exhaustively, but rather primarily address two approaches (together with other topics related to variability.)

1.3.1 Controlled Pressure Method

Most buildings are naturally depressurized relative to atmosphere due to the operation of heating, ventilation, and air conditioning systems, and the so-called stack effect, a topic that will be covered in greater detail in Chapter (TBD). This depressurization induces a flow of air from soil into the building; this flow can carry contaminant vapors into the building. (This view is rather simplistic, as will be discussed throughout this work, but suffices for now.) Using this idea, the controlled pressure method (CPM) was suggested, where blowers are used to control the depressurization of the building, and thereby more effectively controlling the indoor environment. The basic ideas was to create a "worst case" scenario in which contaminant soil vapors are induced to enter the building.

Within the CPM framework, overpressurizing a building will then prevent contaminant entry from occurring. Thus, this can be used to identify indoor contaminant sources, as the presence of any contaminant vapors in the indoor environment in the overpressurized building have to originate from such a source. This approach can be applied as needed and hopefully will reduce the uncertainty and difficulty of VI investigations[**mchugh˙evaluation˙2012**].

1.3.2 Indicators, Surrogates, & Tracers

The conventional sampling schemes currently employed, due to the spatial and temporal variability of VI, has a propensity for creating false positives and negatives. While one solution to this problem is to increase the scope of VI investigations of a particular site, by for instance continuously monitoring the indoor contaminant concentration or by collecting an increasing number of samples, this approach is not practical, especially when numerous sites are involved. Thus, there is a need to develop guidelines that help reduce the sampling requirements and scope of VI investigations, while retaining the same degree of confidence that the relevant level of VI has been determined[**schuver˙chlorinated˙2018**].

To achieve this, it has been suggested to use indicators, surrogates, and tracers (ITS) to determine when to conduct a VI site investigation. For example, can me-

teorological ITS be used to determine when VI is expected tp be the largest, e.g. at which temperature and barometric pressure is, for instance, the 95th percentile indoor contaminant concentration most likely to be found[**schuver˙chlorinated˙2018**]? This is a promising approach, because as we have already discussed, many VI sites have the highest indoor contaminant concentration during colder seasons. So far this is more of a qualitative observation rather than quantitative guidelines for use in VI site investigations.

1.4 Issues With Applying CPM & Using ITS

On the surface, the CPM and ITS methods are two different approaches that try to address the same problem. However, they both attempt to utilize some external variable, such as building pressurization, and either manipulate it directly, or by inference, to determine or predict the indoor contaminant concentration.

The issue with these approaches is that they assume that different VI sites will respond comparably to these external variables, which in reality is not the case. **guo˙identification˙2015**[**guo˙identification˙2015**] used CPM to (inadvertently) identify a preferential pathway at their site, closed it, and noticed a markedly different relationship between indoor contaminant concentration and building pressurization for the period before and after the closing of the preferential pathway.

The reason for this change in behavior will be elaborated on in Chapter (TBD), but consider that contaminant transport from soil into a building across a foundation breach occurs through two means - diffusion and advection. If advective transport dominates, then one would expect a strong correlation between building pressurization and contaminant entry rate, which determines the indoor contaminant concentration; if diffusive transport dominates, this relationship would be absent or weak.

Thus, to reliably apply any technique such as CPM or to use ITS, one needs a good mechanistic understanding of how, for instance, contaminant transport occurs at a VI site, and how the various site specific characteristics give rise to different transport phenomena. Assessing this in the field can be challenging, and therefore we turn to the use of numerical models of VI scenarios, guided by a first-principles perspective, which gives the ability to study physical phenomena in great detail.

1.5 Mathematical Modeling of Vapor Intrusion

Early in the history of VI, mathematical models of VI were formulated to aid investigators and regulators predict human exposure risk. Most of these adapted work done by **nazaroff˙predicting˙1988**[**nazaroff˙predicting˙1988**] who had developed mathematical models of radon intrusion. Perhaps one of the more well-used VI models was the one developed by Johnson and Ettinger in 1991[**johnson˙heuristic˙1991**]. This analytical model could be used to describe the transport of various VI contaminants from a groundwater source into the overlying building, and it was quickly adopted by the EPA as a spreadsheet tool that has seen widespread use since[**u.s.˙environmental˙prote**
Over time more advanced numerical models were developed, which allowed for more physics and VI scenarios to be modeled in greater detail. Some notable examples are the work by **abreu˙effect˙2005**[**abreu˙effect˙2005**] and **pennell˙development˙2009**[**pennell˙develo**

A benefit of using models in VI, besides as a predictive tool, is that their use allows the user to inspect in detail the role that various physics plays in determining VI. In a field that is dominated by empirical field studies of VI sites (which are environments that are difficult to control), models are an invaluable tool that help deepening our understanding of the VI phenomena. Already these have been used to investigate topics such as the role of soil moisture in VI transport[**shen˙influence˙2013**], how different foundation features affect contaminant entry[**yao˙simulating˙2013**], or how wind affects building air exchange with the outdoor and pressurization[**shirazi˙three-dime**

In this work, we will likewise use numerical models, in combination with analysis of field-data from well-studied VI sites to explore the nature of contaminant transport. Some specific topics that will be covered include analysis of how preferential pathways can fundamentally change contaminant transport, and how the lessons learnt can be used to aid in resolving some of the issues in VI investigations, and broaden our understanding of the temporal and spatial variability at VI sites. The role that sorption of contaminant vapors on soils and in the indoor environment, a largely unstudied phenomena, will also be explored, and some of the implications discussed.

1.6 Outline

Note: I purposely left this blank and this section will be completed once the rest of the chapters are done. But a (very) brief summary of what each chapter will cover will be presented here.

Chapter 2

Numerical Modeling of Vapor Intrusion

Abstract

Vapor intrusion (VI) investigations, the effort to determine the exposure and associated human health-risk at a VI impacted building, are often complicated by significant spatial and temporal variability in concentrations of contaminants of concern. Over the years there have been efforts to develop new techniques and methodologies that aim to reduce the uncertainties associated with these variabilities. The goal is to simplify and improve the robustness of VI site investigations. The development of the controlled pressure method (CPM), where the pressurization of a building is controlled in an effort to increase or decrease contaminant entry into the building, is one such example. Another approach is to use indicators, tracers, and surrogates (ITS) to help guide when to conduct site investigations, ideally increasing the likelihood of determining the maximum indoor contaminant concentrations.

Both of these approaches rely on a quasi-deterministic relationship between some external variable, such as building pressurization, and indoor contaminant concentration. However, site-specific conditions can give rise to very different responses to such an external variable. To effectively use CPM or ITS, a better mechanistic understanding of contaminant transport and exposure is needed.

In this thesis, we develop three-dimensional finite element models of VI impacted buildings from a first principles perspective. These models combined with analysis of field data from VI sites, allows us to explore the physical mechanisms that drive VI. By considering the dominant contaminant transport mechanism at a site, e.g. if advective or diffusive transport dominates, we can explain why a change in building pressurization can lead to differences in contaminant concentration variability at different sites. We can also better understand how the various factors governing VI contribute to the overall variability.

By classifying the dominant contaminant transport mechanism at a site, we can more effectively anticipate how a particular site will respond to some external stimuli. This will in turn reduce the effort required to, and increase the robustness of the techniques used determine the relevant human exposure at a VI site.

2.1 Introduction

To formulate a mathematical description of VI, we consider a simple hypothetical VI scenario at steady-state and develop a three-dimensional model of this. Consider a VI impacted house with a 10 m by 10 m foundation footprint with a basement whose foundation lies 1 m below ground surface (bgs). There is also a 1 cm wide crack along the perimeter of the 15 cm thick foundation slab, where all contaminant vapor entry into the house is assumed to occur. Here we will consider the basement alone as the control volume for which the indoor contaminant concentration will be determined. It is assumed to have a ceiling height of 3 m, giving a total volume of $300\,\mathrm{m}^3$ and that contaminant vapors are expelled via air exchange with the exterior of the house; the air exchange rate with outdoor air is assumed to be $0.5\,\mathrm{h}^{-1}$.

The contaminant source be the underlying groundwater, which is assumed to be 4 m bgs, and it is infinitely and homogenously contaminated with TCE (we will normalize everything to this source concentration, so the value does not matter), i.e. the groundwater contaminant concentration does not change over time nor does it have any concentration gradients. We will only consider contaminant transport in the portion of soil between the open ground surface and the groundwater interface - the *vadose zone*. This soil is assumed to be homogenous and consist only of *sandy loam* type soil, i.e. there no soil layers, rocks, etc. For now, we will assume that no contaminant sorption into/onto the soil occurs, but this phenomena will be explored in Chapter (TBD).The house is assumed to be surrounded by open ground that extend 10 m from the house wall. Contaminant concentration in the atmosphere is assumed so low that is effectively zero, i.e. contaminant vapors that reach the ground surface are immediately infinitely diluted.

The house interior is assumed to be slightly depressurized relative to ambient due to the stack effect; the indoor/outdoor pressure difference is $-5\,\mathrm{Pa}$ This induces an airflow from the ground surface, through the soil, and into the house via the foundation crack. The airflow interacts with contaminant diffusion in the soil. Figure 2.1 shows a figure summarizing this VI scenario.

The basement interior will be modeled as a continuously stirred tank reactor (CSTR), (but without reactions), where the indoor contaminant concentration will depend on the contaminant entry rate n_{ck} from the soil via the foundation crack and the air exchange rate A_e. The details of this will be covered section 2.3.1.

To determine n_{ck} the contaminant transport in the soil needs to be modeled. This will be done using the advection-diffusion equation, which will be modified for transport in soils. The contaminant transport itself is driven by a concentration gradient and airflow in the soil. The contaminant source (groundwater) and sink (atmosphere and contaminant entry into the building) will largely determine the concentration gradient, while the airflow needs to be calculated separately.

The airflow in the soil is modeled by Darcy's Law, and is driven by a pressure gradient in the soil, which induced by the indoor/outdoor pressure difference. Details are in section 2.3.3.

One last consideration is that the vadose zone is partially saturated with water, with the soil pores more or less filled near the groundwater interface, and with soil moisture content decreasing as a function of elevation above groundwater z [m]. The soil moisture content has a profound effect on transport in the soil; it restricts both the airflow and contaminant diffusivity in the soil. Thus, the soil moisture content

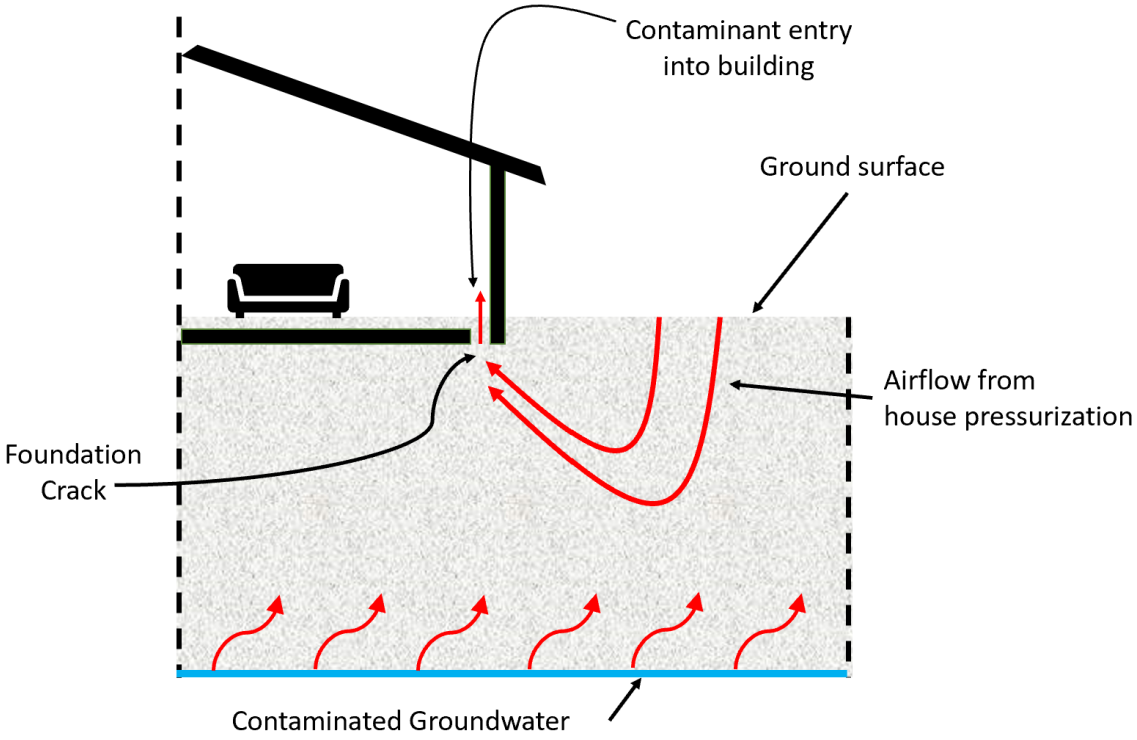

Figure 2.1: The considered VI scenario.

θ_w must first be determined in order to solve the contaminant transport and Darcy's Law.

The resulting physical system is highly coupled, with many physical aspects dependant on others. Figure 2.2 shows the coupling between each physicsal process, its output, and how it relates to the other processes that ultimately determine VI.

In this chapter, we will walk through the process of numerically modeling this VI scenario using the finite element method (FEM) and post-processing of the results. A discussion regarding past and present VI models, their advantages and limitations, will follow.

2.1.1 Finite Element Method

Many physical phenomena are described by partial differential equations (PDEs), but for anything but the simplest scenarios, these do not have an analytical closed-form solutions; therefore numerical methods are needed for finding an approximate solution. This is achieved by discretizing the problem, i.e. transforming a continuous problem into a discrete one. There are numerous ways to discretize a problem, and some of the more popular schemes are finite difference (FDM), finite volume (FVM), and finite element method (FEM).

In this work we use FEM, which is a popular numerical scheme that offers some distinct advantages over other schemes for modeling VI. FEM subdivides the domain of the PDE problem into many smaller subdomains called elements. These elements can take a wide variety of shapes, e.g. tetrahedra, prisms, or cuboids for three-dimensional problems and triangles or rectangles for two-dimensional problems. The collection of elements that make up the domain or geometry is called a *mesh*. The

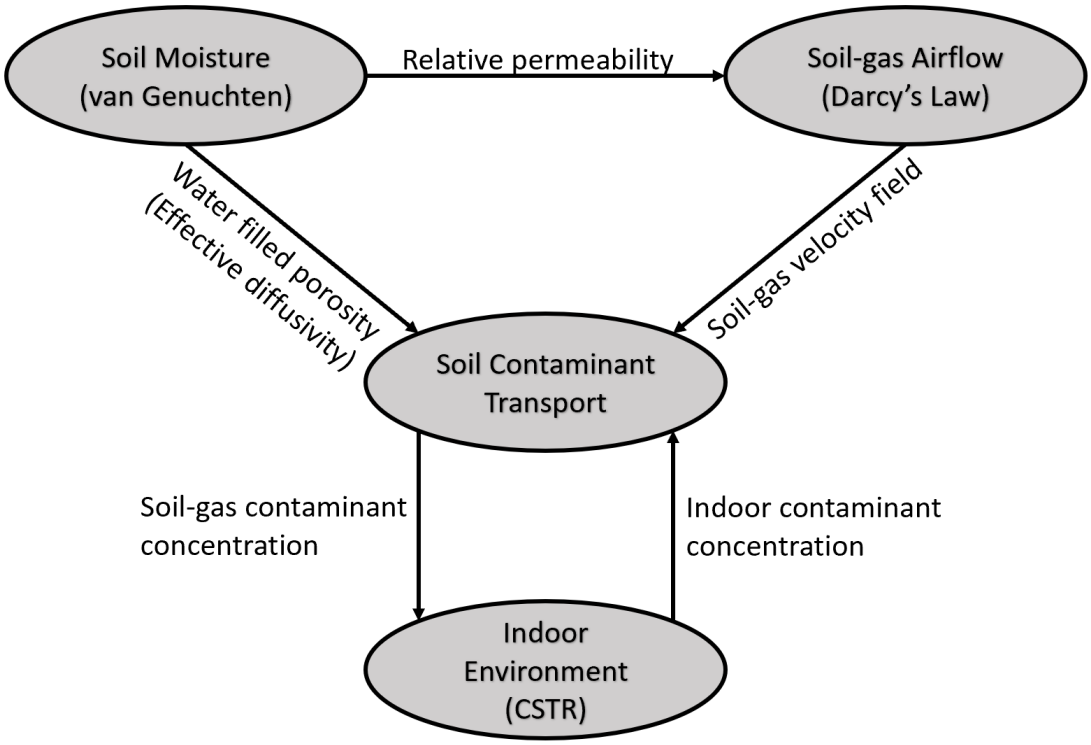

Figure 2.2: Coupling between the physics used to model VI.

fineness of the mesh is what largely determines the accuracy of the solution, but also increases the computational costs.

The size of each element can be highly nonuniform which allows FEM to discretize complicated geometries. This is advantageous for modeling VI, where different parts of the geometry can have dramatically different resolution requirements; the 1 cm foundation crack requires elements on the scale of mm, while in other parts of the geometry the resolution requirement is on the scale of m. This ability to easily represent complicated geometries with elements of ununiform sizes helps maintain accuracy while saving computational resources. Another benefit of using these elements is that it is easy to assign different constant values throughout the domain, and heterogenous materials can easily be represented.

The purpose of this work is not to provide a detailed description of the FEM, but for the interested reader **larson˙finite˙2010**[**larson˙finite˙2010**] is a good resource. However, it is important to know that FEM assumes that the approximated solution to a PDE can be written as a series of linear functions, called *basis functions*.

$$u \approx u_h = \sum^{i} u_i \psi_i \tag{2.1}$$

here u is the exact solution to the problem; u_h is the approximate solution; u_i is a *nodal coefficient*; and ψ is a *basis function*. These basis functions are usually some simple function, e.g. a hat function or some lower-order polynomial.

These basis functions are used to discretize the problem by rewriting a PDE into its *weak form*, multiplying the equation with another set of functions called a *test function*. The test functions are the same type of function as the basis function, i.e. if the basis function is a hat function, so is the test function. The result of this is an

integral, where the integrands are the product of the basis function. These integrals are numerically solved using some quadrature method, which gives a linear system of equations. This system of equations is then solved to give all of the u_i coefficients and thus the approximated solution u_h.

The point of this is that choice of basis function, i.e. hat function, first or third order polynomial, can influence the accuracy of the solution, and certain basis functions are more appropriate for certain PDEs. Generally, higher order polynomials will give a more accurate solution, but at a computational cost, making it sometimes difficult to choose. This adds another level of complexity of using FEM over some other numerical schemes, as the accuracy of the solution is not only influenced by the mesh but also somewhat by the choice of basis functions. This highlights one of the drawbacks of FEM, i.e. that it is mathematically more challenging to implement and use than some other numerical schemes may be.

Fortunately, due to the attractiveness of the method, many commercial FEM packages have developed which increases usability significantly. In this work we will use such a package - COMSOL Multiphysics, where subsequent sections will cover the steps required to implement our VI model in COMSOL. (Of course, this could easily be translated into use in another software package.)

In order, we will cover:

1. Creation of a model geometry.
2. Defining physics/governing equations, boundary, and initial conditions.
3. Discretize/mesh the geometry.
4. Solver configuration.
5. Post-process the results.

2.2 Geometry Generation

Designing a good model geometry is critical as it can save significant computational resources. When designing a geometry the FEM user should try to represent the model geometry as accurately as possible while:

1. Avoid unnecessarily fine details; these may require an excessively fine mesh to resolve.
2. Leverage symmetry to reduce geometry size and thereby the mesh.

Achieving these goals is not always straightforward, and depend on the skill of the modeler and on the available tools. Typically a model geometry is constructed in some computer assisted design (CAD) software, and the particular tools available in these vary by software.

COMSOL has a built-in geometry generation tool, which allows the construction of advanced geometries by performing various operations on simpler geometries, e.g. a cylinder and half sphere can be combined to make a rivet. It is also possible to import pre-generated geometries from other CAD software. However, we will create our own geometry.

The interior of the house itself will not be explicitly modeled, instead we only consider the soil surrounding the house. This is done for the simple reason that it is not important to do so. Once the contaminant is in the structure, that is the key consideration. In addition, interiors are simply too heterogenous to generalize in any meaningful way. If the interior was explicitly modeled to offer insights into indoor concentration variations, it would be prohibitively expensive to do, as it would require solving the Navier-Stokes equation. Instead the interior is implicitly modeled as a CSTR and simply coupled with the explicit soil and foundation geometry via the foundation crack boundary.

One of the nice properties of our VI scenario is that, due to symmetry, we only need to explicitly model a quarter of it. This reduces the number of required mesh points by 75%, which is a huge computational saving. To create the specified geometry, see the instructions for geometry generation in the appendix.

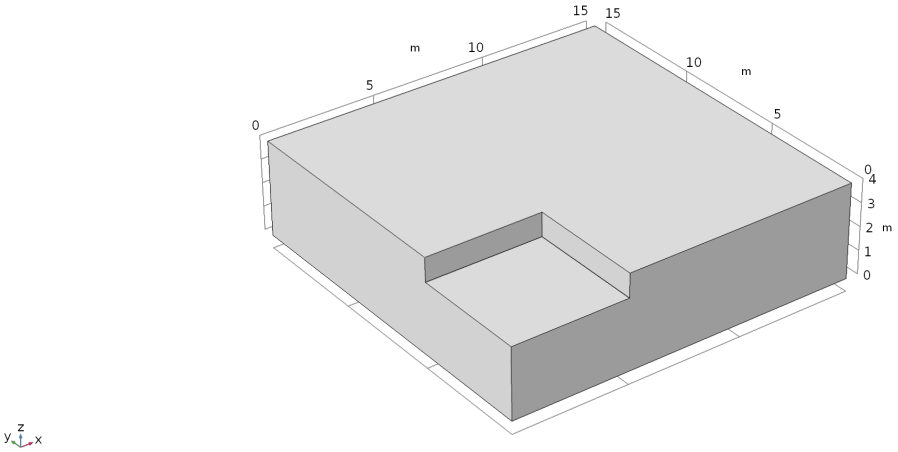

Figure 2.3: The complete geometry of the VI scenario.

2.3 Vapor Intrusion Physics & Govering Equations

2.3.1 The Indoor Environment

The impacts on the indoor air space is perhaps the most important part of modeling VI, as the goal of these models ultimately is to predict indoor exposure given some external factors. The indoor environment is, however, only modeled implicitly as a continuously stirred tank reactor (CSTR).

We assume that all contaminant entry into the house occurs via the foundation crack. Once the contaminant enters the interior, it is instantly perfectly mixed, which is a key assumption of a CSTR. Contaminant expulsion occurs via air exchange with the outdoor environment, and is regulated by *air exchange rate* A_e, which dictates what fraction of the indoor air is exchanged with outdoor air over a given period of time. For instance, a common air exchange rate for a house is $0.5\,\mathrm{h}^{-1}$, i.e. half of the indoor air is exchanged every hour. It should be noted that in this simple VI model implementation, we assume that there are no indoor sources nor that any

sorption of contaminant to/from any indoor materials occurs. Thus, the reaction term that would ordinarily be part of a CSTR is dropped (but is reintroduced in Chapter (TBD)) and the change in indoor contaminant concentration is thus given by (2.2).

$$V_{\text{bldg}} \frac{\partial c_{\text{in}}}{\partial t} = n_{\text{ck}} - V_{\text{bldg}} A_e c_{\text{in}} \tag{2.2}$$

Here c_{in} [$\text{mol}\,\text{m}^{-3}$] is the indoor air contaminant concentration; n_{ck} [$\text{mol}\,\text{s}^{-1}$] is the contaminant entry (or exit) rate into the building via the foundation crack; $A_e = 0.5\,\text{h}^{-1}$ is the air exchange rate; Finally, $V_{\text{bldg}} = 300\,\text{m}^3$ is the volume of the house interior (or basement in this case).

A limitation of this approach is that we only consider one control volume or compartment, while in reality indoor contaminant concentrations can vary significantly between compartments, in particular between different floors. There are VI models that use multiple compartments, which in essence are just coupled CSTRs[**murphy˙multi-compartment˙2011**]. Basements typically have higher indoor contaminant concentrations than other floors, so in this implementation we assume that our sole compartment is the house basement, which $V_{\text{bldg}} = 300\,\text{m}^3$ reflects.

Solving (2.2) requires us to determine the contaminant entry and air exchange rates. Air exchange rates can vary quite significantly, and are a significant source of temporal variability in VI, a topic that will be further explored in Chapter (TBD). However, they typically vary around relatively well-known values as air exchange rates are regulated in building codes. For residential buildings, it is typical that air exchange rate is around $A_e = 0.5\,\text{h}^{-1}$ and thus for simplicity we will choose this value.

Contaminant entry into the building Contaminant entry rates are significantly more difficult to determine, as they depend on air velocity through the foundation breach and the concentration gradient across it. The determination of these is the main point, and challenge in VI modeling.

The contaminant entry n_{ck} is given by integrating the contaminant entry flux j_{ck} across the foundation crack boundary A_{ck}.

$$n_{\text{ck}} = \int_{A_{\text{ck}}} j_{\text{ck}} dA \tag{2.3}$$

The contaminant flux through the foundation crack is modeled as transport between two parallel plates and has an advective and a diffusive component.

$$j_{\text{ck}} = j_{\text{advection}} + j_{\text{diffusion}} \tag{2.4}$$

Since contaminant concentration indoors is lower than it is in the soil or near foundation crack region a concentration gradient from the soil-gas to the indoor will exist. The interior of the crack is not explicitly modeled, but assumed to only contain air and thus we assume the diffusion coefficient is the same as in air.

$$j_{\text{diffusion}} = -\frac{D_{\text{air}}}{L_{\text{slab}}}(c_{in} - c_g) \tag{2.5}$$

here $D_{\text{air}} = 7.2 \times 10^{-6}\,\text{m}^2\,\text{s}^{-1}$ is the diffusion coefficient of TCE in air as a sample contaminant of interest; other contaminant of common concern have comparable

diffusivities. $L_{\text{slab}} = 15\,\text{cm}$ is the thickness of the foundation slab; c_{in} [$\text{mol}\,\text{m}^{-3}$] is the indoor contaminant concentration; c_g [$\text{mol}\,\text{m}^{-3}$] is the contaminant gas-phase concentration at the foundation crack boundary.

Advective transport through the slab can occur in both directions, i.e. contaminants can be carried from the soil into the house and from the house into the soil[**holton˙creation˙2018**]. The direction of this transport depend on the direction of the flow, with a positive sign indicating that airflow goes into the house.

$$j_{advection} = \begin{cases} u_{ck}c_g & u_{ck} \geq 0 \\ u_{ck}c_{in} & u_{ck} < 0 \end{cases} \tag{2.6}$$

here u_{ck} [$\text{m}\,\text{s}^{-1}$] is the airflow velocity through the foundation crack.

Thus the total contaminant transport through the foundation crack is given by (2.7).

$$j_{ck} = \begin{cases} u_{ck}c_g - \frac{D_{\text{air}}}{L_{\text{slab}}}(c_{in} - c_g) & u_{ck} \geq 0 \\ u_{ck}c_{in} - \frac{D_{\text{air}}}{L_{\text{slab}}}(c_{in} - c_g) & u_{ck} < 0 \end{cases} \tag{2.7}$$

Not only will (2.7) be used to calculate the contaminant entry rate into house, but is a necessary boundary condition for calculating the contaminant concentration in the soil. However, as we see, (2.7) is a function of both the soil-gas concentration at the foundation crack boundary c_g and the indoor contaminant concentration cin, thus these two are coupled and needs to be solved simultaneously.

2.3.2 Variable Soil Moisture Content

The portion of soil between groundwater and ground surface is variably saturated with water and is called the vadose zone. Under environmental conditions, TCE and many other contaminants are miscible in water, and will be partitioned between its dissolved and vapor phases, which has profound effects on the total contaminant transport in the vadose zone. The rates of diffusion in liquids and gases usually differ by orders of magnitudes. Likewise, advective transport in the two phases are vastly different, and as such it is important to account for the varying soil moisture content.

Water filling of soil pores from groundwater is driven by a negative pressure gradient induced by surface tension, called capillary potential and is here represented by ψ. This capillary potential is a function of the soil moisture content, and becomes increasingly negative as the water content decreases, and is zero when the soil matrix is saturated with water. The capillary potential varies with the hydraulic properties of specific soil types.

In addition to the capillary potential, soil moisture content is driven by a gravitational potential, e.g. groundwater flow in soil. The total soil moisture potential ϕ, is the sum of the capillary and gravitational potentials, here expressed as a pressure head.

$$\phi = \frac{\psi(\theta_w)}{\rho g} + h_{\text{g}} = h + h_{\text{g}} \tag{2.8}$$

where ϕ [m] is the total soil moisture potential (as a pressure head); ψ [Pa] is the capillary potential; h [m] is the capillary potential as a pressure head above the groundwater/soil interface; θ_w is the volumetric moisture content by volume soil,

i.e. dimensionless; ρ [kg m^{-3}] is the density of water; g [m s^{-2}] is the acceleration due to gravity; and h_g [m] is the gravitational potential above a reference plane.

In the VI scenario considered here, we assume that there is no gravitational potential, and thus that the soil moisture content is at steady-state. This simplifies the determination of the soil moisture content, which now is entirely determined by the capillary potential ψ, or h in our case.

There are two common methods for modeling the capillary potential, one developed by **brooks˙properties˙1966**[**brooks˙properties˙1966**] in 1966, and another by **van˙genuchten˙closed-form˙1980**[**van˙genuchten˙closed-form˙1980**] in 1980. Both of these are semi-empirical approaches and relies on experimentally determined parameters for a specific soil type to be used. In this work, we only use van Genuchten's method, simply because parameters for a wide variety of soils have been made available by the EPA and may be seen in Table 2.

If the assumption that there is no gravitational potential cannot be made, then the full soil moisture potential ϕ needs to be determined. This is achieved by solving Richard's equation.

van Genuchten's Soil-Water Retention Model

The relationship between capillary pressure and moisture content is called *soil moisture retention*, and is what van Genuchten's method models. Specifically, his method models the water saturation of the soil and is given by (2.9).

$$\mathrm{Se} = \begin{cases} \frac{1}{(1+(\alpha|h|)^n)^m} & h < 0 \\ 1 & h \geq 0 \end{cases} \tag{2.9}$$

here Se is the saturation, which ranges from 0 to 1, where 1 is fully saturated with water; α, m, and $n = \frac{1}{1-m}$ are the empirically determined van Genuchten parameters and can be seen in Table 2; and h [m] is the capillary pressure head, which in this case is the elevation above the groundwater/soil interface.

It is important to note that $\mathrm{Se} = 0$ does not mean that there is no moisture in the soil, but soils retain a small amount of water in the matrix - residual moisture content (which again is soil specific). Thus, the soil moisture content is given by (2.10)

$$\theta_w = \begin{cases} \theta_r + \mathrm{Se}(\theta_t - \theta_r) & h < 0 \\ \theta_t & h \geq 0 \end{cases} \tag{2.10}$$

where θ_w is the volumetric soil moisture content; θ_t is the soil porosity; and θ_r is the residual moisture content.

By extension, the soil gas or air content is given by

$$\theta_g = \theta_t - \theta_w \tag{2.11}$$

An example of the soil saturation and moisture content as a function of pressure head is shown in Figure 2.4. Note the steep decline in moisture content near the groundwater interface - that is the capillary zone and we will see that it presents a significant barrier to contaminant transport from the groundwater in section 2.3.4.

The presence of water in the soil matrix has profound implications for transport as the pore space may be restricted to only one phase. For instance, in the capillary

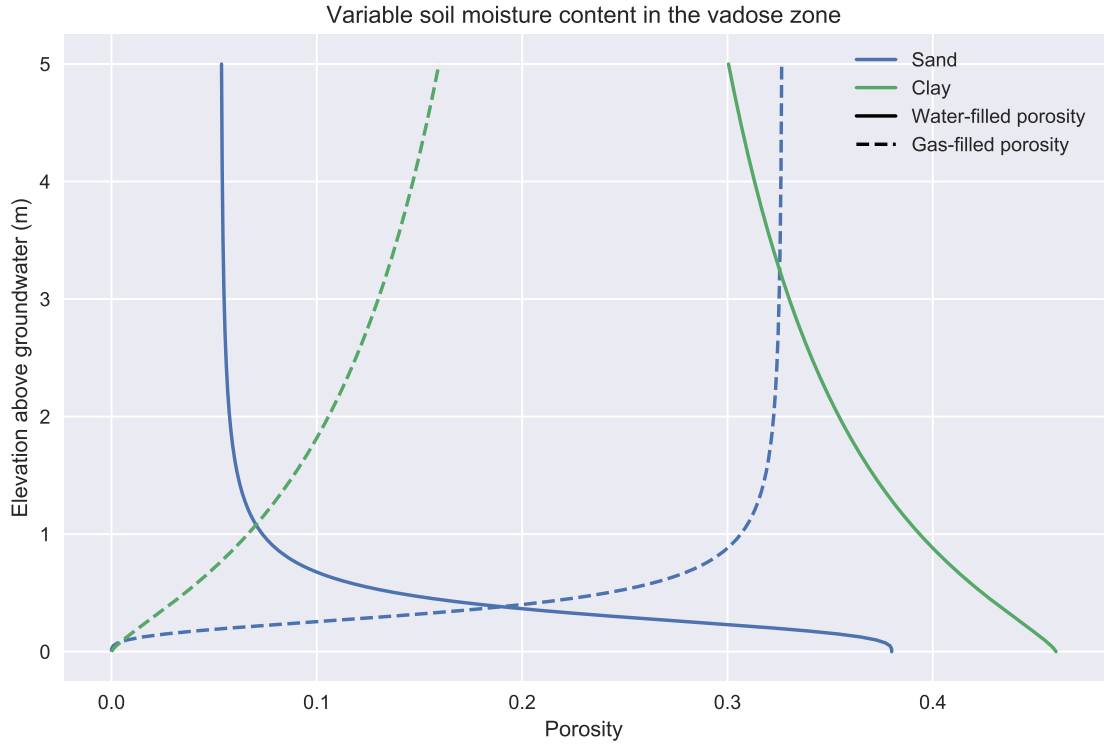

Figure 2.4: Example of a soil moisture retention curve as a function of pressure head above the groundwater/soil interface.

zone, the only possible bulk transport in the water phase, while gas phase transport is impossible. The opposite is true near the ground surface, where most of the pore space consists of air.

Soil already limits transport for a single phase due to its permeability, i.e. it is harder to pump water through a soil columns than a pipe of the same size. This extra phase-specific transport inhibition is modeled as a *relative permability* and is given by (2.12).

$$k_r = \begin{cases} \mathrm{Se}^l \left[1 - \left(1 - \mathrm{Se}^{\frac{1}{m}}\right)\right]^2 & h < 0 \\ 0 & h \geq 0 \end{cases} \tag{2.12}$$

here k_r is the relative permeability for water; and $l = 0.5$ is another van Genuchten parameter.

The relative permeability varies from 0 to 1, where 0 indicates that the soil matrix is completely impermeable to the fluid, while a value of 1 means that there is no additional permeability cost. Since k_r here is relative to water, the gas phase relative permeability is given by $1 - k_r$. Figure 2.5 shows how the relative gas and water permeability varies in the vadose zone.

2.3.3 Airflow In The Vadose Zone

In our VI scenario, the depressurized house induces an advective airflow from the ground surface, through the vadose zone, and into the house via the foundation crack, carrying contaminant vapors with it. This airflow is modeled using a modified version of Darcy's Law. The modification is made to account for the variable

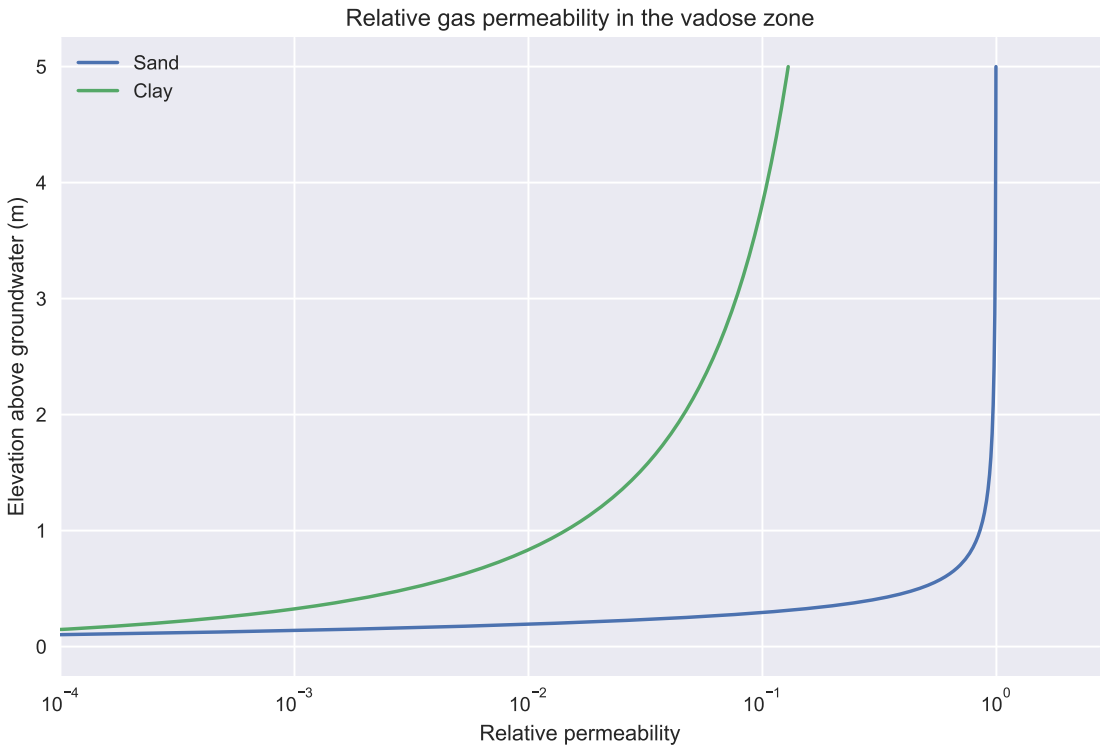

Figure 2.5: Relative gas and water permeability in the vadose zone or above the groundwater interface.

moisture content in the vadose zone, which is established in section 2.3.2.

Darcy's Law describes the flow of a fluid through a porous medium. This flow is driven by a pressure gradient, and its magnitude depends on the permeability of the porous medium and the fluids viscosity.

$$\vec{u} = -\frac{\kappa}{\mu}\nabla p \tag{2.13}$$

here $\vec{u}$ [$\mathrm{m\,s^{-1}}$] is the airflow velocity vector; κ [$\mathrm{m^2}$] is the permeability of the porous media; μ [$\mathrm{Pa\,s}$] is the dynamic viscosity of the fluid; and ∇ [$\mathrm{Pa\,m^{-1}}$] is the pressure gradient.

This (2.13) formulation of Darcy's Law assumes that the porous media is saturated with the fluid,[1] hence the need to modify this expression. While porosity is not directly part of (2.13), it is an intrinsic property of the permeability κ of the porous media; the variably saturated pores variably changes the permeability. This variation in permeability is modeled using the relative permeability expression from van Genuchten's equation (2.12). The effective soil permeability is the product of the soil permeability and its relative permeability giving our modified Darcy's Law (2.14).

$$\vec{u} = -\frac{(1-k_r)\kappa}{\mu}\nabla p \tag{2.14}$$

[1]Darcy's Law also assumes that the flow is in the laminar regime, i.e. the Reynolds number $\mathrm{Re} < 1$. Due to the small pressure gradients in most VI scenarios, this assumption is rarely unfulfilled, but if it is, then Brinkman's equation should be used instead.

Recall that by definition k_r is the relative permeability of the soil to *water* and thus $1 - k_r$ is that to *gas*.

To calculate the soil-gas velocity field in the vadose zone, we need a continuity equation, which for fluid flow is (2.15).

$$\frac{\partial \rho}{\partial t} + \nabla \cdot (\rho \vec{u}) = 0 \tag{2.15}$$

Inserting our modified Darcy's Law for the velocity gives (2.16).

$$\frac{\partial}{\partial t}(\rho \theta_g) + \nabla \cdot \rho \Big(- \frac{(1 - k_r)\kappa}{\mu} \nabla p \Big) = 0 \tag{2.16}$$

where θ_g is the gas-filled porosity of the soil from (2.11); $\rho = 1.225\,\mathrm{kg\,m^{-3}}$ is the density of air; and $\mu = 18.5 \times 10^{-6}\,\mathrm{Pa\,s}$ is the dynamic viscosity of air. Contaminant vapor concentrations are typically highly dilute in VI scenarios, and therefore we assume that the contaminant does not affect the transport properties of air.

In order to solve (2.16) we need to define some boundary conditions. In our CSM, air is pulled from the atmosphere through the ground surface and into the building via the foundation crack. To model this only three boundary conditions are required.

Boundary Conditions The first is to define a pressure gauge, i.e. a reference point for where the pressure is zero, which is where air will be pulled from. This is the applied to the ground surface boundary. The second is that we apply the indoor/outdoor pressure difference (-5 Pa) to the foundation crack boundary. The third type is applied to all remaining boundaries and is a no flow boundary condition, indicating that no flow passes through these boundaries. We also make sure that we specify the symmetry planes present.

Ground surface	$p = 0\,\mathrm{Pa}$	(2.17)
Foundation crack	$p = p_{\mathrm{in/out}} = -5\,\mathrm{Pa}$	(2.18)
Remaining	$-\vec{n} \cdot \rho \vec{u} = 0$	(2.19)

where $\vec{n}$ is the boundary normal vector.

Initial Conditions For steady-state problems, the initial conditions do not influence the solution. Transient simulations however, require initial conditions and these are assumed to be given by the steady-state solution.

Basis function A hat function is used as the basis function for solving Darcy's Law in FEM.

2.3.4 Mass Transport In The Vadose Zone

To begin deriving a governing equation for contaminant transport in our VI scenario, we consider the continuity equation which states that the change of concentration in some volume of space depends on the advective and diffusive fluxes in and out of the system, as well as any generation or consumption inside the system.

$$\frac{\partial c}{\partial t} + \nabla \cdot (j_{\mathrm{adv}} + j_{\mathrm{diff}}) - G = 0 \tag{2.20}$$

here c [mol m^{-3}] is the concentration of the chemical species; t [s] is time; j_{adv} and j_{diff} [mol s^{-1} m^{-2}] are the advective and diffusive fluxes respectively; and G [mol s^{-1}] is the generation or consumption of the chemical species.

In our model we will assume that $G = 0$ as the groundwater is the sole contaminant source and TCE does not readily degrade in soils. However, this term should remain and an appropriate expression developed if one wants to model:

- Biodegradation of some compound in the soil.
- Radon intrusion (remember radon gas is generated in soils and rocks).
- A soil or subsurface source, e.g. a leaky tank or evaporation from a (pure) contaminant spill.

The advective flux is given by

$$j_{\text{adv}} = \vec{u}c \tag{2.21}$$

where $\vec{u}$ [m s^{-1}] is a velocity vector. The diffusive flux is given by Fick's Law

$$j_{\text{diff}} = -D\nabla c \tag{2.22}$$

where D [m^2 s^{-1}] is the diffusion coefficient of the contaminant in the solute; and ∇c [mol m^{-3} m^{-1}] is a concentration gradient. Thus we get the advection-diffusion equation which generally governs transport of a chemical species

$$\frac{\partial c}{\partial t} + \nabla \cdot (\vec{u}c + -D\nabla c) = 0 \tag{2.23}$$

However, this will not accurately represent contaminant transport in the vadose zone due to

- Contaminant transport occurs inside a variably saturated porous matrix, significantly affecting transport properties.
- The contaminant concentration in the vadose zone will be distributed between three phases - gas, water, and solid (via sorption).

The total contaminant concentration in the soil will be used in lieu of just concentration, i.e. $c \to c_T$ and thus the total contaminant concentration is the sum of the gas, water, and solid phase concentrations.

$$c_T = \theta_w c_w + \theta_g c_g + c_s \rho_b \tag{2.24}$$

Here θ_g and θ_w are the gas-filled and water-filled porosities respectively; c_w and c_g [mol m^{-3}] are the contaminant concentrations in water and gas respectively; c_s [mol kg^{-1}] is the solid phase or sorbed concentration per mass of soil; and $\rho_b = (1 - \theta_t)\rho$ [kg m^{-3}] is the bulk density of the soil, which can be calculated from the soil porosity θ_t and solid phase density of the soil ρ [kg m^{-3}].

The attentive reader will now notice that our governing equation depend on three variables instead of one. However, remember that we're concerned with low contaminant concentrations, we can relate the gas and liquid phase concentrations via Henry's Law (2.25)

$$c_g = K_H c_w \tag{2.25}$$

where $K_H = 0.402$ is the dimensionless Henry's Law constant for TCE at 20 °C. We also assume that there are no temperature gradients throughout the vadose zone.

The solid phase concentration can be related to the others via a linear sorption isotherm. Here either the gas-solid or water-solid sorption interaction can be chosen; the former is used in Chapter (TBD) to we will explore effect of gas-solid sorption.

$$c_s = \begin{cases} K_p c_w & \text{Water-solid sorption} \\ K_p c_g = K_p K_H c_w & \text{Gas-solid sorption} \end{cases} \tag{2.26}$$

here K_p [$\mathrm{m^3\,kg^{-1}}$] is a sorption partitioning coefficient.

Another approach is to simply ignore the role of sorption completely, i.e. $K_p = 0$, which has historically been done in VI modeling and is done in this example too. The reason for this is two-fold.

1. Relevant sorption data has not been available.
2. With an infinite source assumption, and at steady-state, sorption doesn't affect the solution; these have been common assumptions in most VI models so far.

Regardless, we will continue with the sorption K_p term, because this will become relevant in Chapter (TBD) where experimentally derived relevant sorption data is available.

With Henry's Law and the linear sorption assumption we can relate the total contaminant concentration in the soil matrix to the water-phase contaminant concentration.

$$c_T = (\theta_w + \theta_g K_H + K_H K_p \rho_b) c_w \tag{2.27}$$

The terms in front of c_w are collected as $R = (\theta_w + \theta_g K_H + K_H K_p \rho_b)$. This term is called the *retardation factor* and reflects the increased contaminant residence time in the matrix due to shifting between the phases, and becomes an important factor in transient transport simulations.

In the vadose zone, advective transport can occur in both the water and gas phases inside the soil pores.

$$j_{\mathrm{adv}} = \vec{u}_{w,pore} c_w \theta_w + \vec{u}_{g,pore} c_g \theta_g \tag{2.28}$$

here $\vec{u}_{w,pore}$ and $\vec{u}_{g,pore}$ [$\mathrm{m\,s^{-1}}$] are the water and gas phase *pore* velocities vectors respectively. However, from mass conservation, we know that the product of the pore velocity and porosity gives the superficial velocity of a fluid in porous media, i.e. the Darcy's Law velocities. This together with Henry's Law gives

$$j_{\mathrm{adv}} = (\vec{u}_w + \vec{u}_g K_H) c_w \tag{2.29}$$

and here $\vec{u}_w + \vec{u}_g$ [$\mathrm{m\,s^{-1}}$] are the Darcy or superficial velocity vectors.

In section 2.3.2 we assumed that there is no gravitational water potential in the soil matrix, and it follows that the water in the pores is stationary, i.e. $\vec{u}_w = 0$ giving

$$j_{\mathrm{adv}} = \vec{u}_g K_H c_w \tag{2.30}$$

where $\vec{u}_g$ is the solution from solving Darcy's Law in section 2.3.3.

To model a scenario where there is a gravitational water potential, one would have to solve two-phase Darcy's Law to get both $\vec{u}_g$ and $\vec{u}_w$. This significantly

complicates the mass transport aspect as well, and as such is beyond the scope of this work.

The diffusive transport expression likewise needs to be adjusted, and the total diffusive flux through the pore matrix is given by

$$j_{\text{diff}} = -(D_w \theta_w \tau_w \nabla c_w + D_g \theta_g \tau_g \nabla c_g) \tag{2.31}$$

here $D_w = 1.02 \times 10^{-9}\,\text{m}^2\,\text{s}^{-1}$ and $D_g = 6.87 \times 10^{-6}\,\text{m}^2\,\text{s}^{-1}$ are the contaminant diffusion coefficients of TCE in pure water and gas respectively; and τ_w and τ_g are the water and gas tortuosity terms.

Due to the irregular shapes of pores, diffusion of a chemical species will inevitably often occur along a tortuous path, which the tortuosity terms attempt to capture. As tortuosity depend on the structure of the porous matrix, it is difficult to accurately portray, but a popular approach is to use Millington & Quirks model[**millington˙permeability˙1961**].

$$\tau_w = \frac{\theta_w^{\frac{7}{3}}}{\theta_t^2},\ \tau_g = \frac{\theta_g^{\frac{7}{3}}}{\theta_t^2} \tag{2.32}$$

here θ_t is the total or saturated porosity of the soil matrix. Another popular approach is Bruggeman's model, or if possible, a custom version can be used.

Combining (2.32) and (2.25) in our diffusion flux expression gives

$$j_{\text{diff}} = -\Big(D_w \frac{\theta_w^{\frac{10}{3}}}{\theta_t^2} + D_g \frac{\theta_g^{\frac{10}{3}}}{\theta_t^2} K_H\Big) \nabla c_w \tag{2.33}$$

the terms in front of ∇c_w can be collected as an effective diffusion coefficient D_{eff} $[\text{m}^2\,\text{s}^{-1}]$, which with our isothermal vadose zone assumption only depends on the soil moisture content. Thus we get the final diffusive flux expression

$$j_{\text{diff}} = -D_{\text{eff}} \nabla c_w \tag{2.34}$$

Figure 2.6 shows how the effective diffusivity varies from being close to that of the pure water diffusivity near the capillary zone, and increases to something closer to gas-phase diffusivity as the soil moisture decreases.

Putting all this together finally gives us the governing equation for contaminant transport in the vadose zone for our modeled VI scenario.

$$R \frac{\partial c_w}{\partial t} = \nabla \cdot (D_{\text{eff}} \nabla c_w) - K_H \vec{u}_g \cdot \nabla c_w \tag{2.35}$$

To solve this we need to define some boundary and initial conditions.

Boundary Conditions In this VI scenario, the sole contaminant source is assumed to be the homogenously contaminated groundwater, which we assume to have a fixed concentration. The atmosphere acts as a contaminant sink and thus this is simply a zero concentration boundary condition. Contaminants leave the soil domain and enter the building through a combination of advective and diffusive

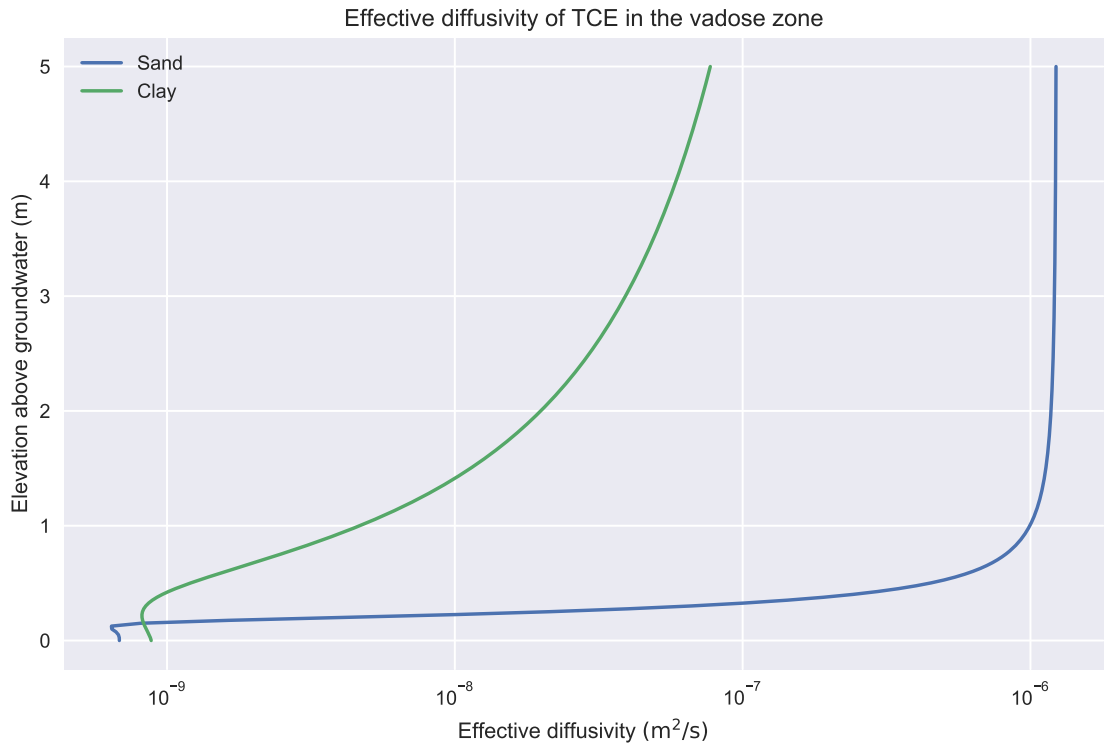

Figure 2.6: Effective diffusivity of TCE in the vadose zone using Millington-Quirks model. Soil water and gas filled porosites are calculated using van Genuchten's equations.

gas phase transport. The boundary condition applied to all other boundaries is a no-flow boundary.

Atmosphere	$c_w = 0\,\mathrm{mol\,m^{-3}}$	(2.36)
Groundwater	$c_w = c_{gw} = 0.1\,\mathrm{mol\,m^{-3}}$	(2.37)
Foundation crack	$-\vec{n} \cdot \vec{N} = \frac{-j_{ck}}{K_H}\,\mathrm{mol\,m^{-2}\,s^{-1}}$	(2.38)
All other	$-\vec{n} \cdot \vec{N} = 0\,\mathrm{mol\,m^{-2}\,s^{-1}}$	(2.39)

$\vec{n} \cdot \vec{N}$ is the dot product between the boundary normal vector and the contaminant flux; j_ck is the contaminant vapor flux into the building. We assume that only contaminants in the gas phase enter the building, and dividing j_{ck} by K_H we get proper accounting in terms of the water phase concentration accounting in the main transport equation 2.35.

Initial Conditions For steady-state problems, the initial conditions do not influence the solution. Transient simulations however, require initial conditions and these are assumed to be given by the steady-state solution.

Basis function A second order polynomial (quadratic) function is used as the basis function for solving the transport equation.

2.4 Meshing

The mesh in FEM model is the collection of small discrete elements make up the model geometry or domain. Meshing is the process of generating a mesh. Meshing is one of the most important aspects of FEM modeling as the mesh directly influences the accuracy of the solution; it is important that the various gradients are resolved by the mesh. However, designing a good mesh can be challenging as a finer mesh has a higher computational cost. A good mesh designer must constantly balance accuracy and computational costs by considering where a mesh can be finer and where it can be coarser.

The most fundamental unit of the mesh is the element(s) that comprise the mesh. There are many different types of elements that can be used for meshing and choosing which ones to use depend primarily on the spatial dimensionality of the model, the particularities of the geometry, and the physics that we wish to model. Obviously different element types are by necessity needed to model a 2D vs. 3D geometry; you cannot mesh a 3D geometry with 2D squares.

There are primarily four types of 3D mesh elements available - the tetrahedral, cuboid, prism, and pyramid. These can be combined in various ways to represent any 3D geometry. The most general 3D element is the tetrahedral and will approximate any geometry well. However, it is not always the most effective choice for meshing a geometry and another element type may be better suited. This is easiest illustrated with an example.

Imagine that you are trying to simulate the laminar flow of some fluid in a pipe. Because of symmetry, only a wedge of the pipe needs to be explicitly modeled. Therefore, in this scenario, it might be beneficial to use prism elements rather than tetrahedrals, since these are already wedge shaped.

The laminar pipe flow is also going to primarily have a gradient in the direction of the flow. Thus the mesh mostly only needs to be fine in the flow direction, while the mesh can be coarser in the orthogonal direction. Constructing a mesh on this basis would allow us to achieve a solution of high accuracy while still keeping the number of elements relatively small - all through clever mesh design.

This is of course a relatively simple example and more complicated geometries may need all kinds of element for constructing a clever design. These type of multi-element meshes can give significant computational saving but at the expense of often requiring significant user input to be generated. Sticking to one type of elements is often simpler as these can quickly and easily mesh geometries.

Meshing can be done manually, but is often performed by a meshing algorithm. The creation of these algorithms is a science in itself, but their use often involve passing some basic parameters to the algorithm. Here the user could, for instance, specify the maximum and minimum element sizes, max element growth rate, how finely small features or curves (typically quite difficult to mesh) should be meshed. These instructions can be specific to various parts of the model, e.g. much finer meshing resolution can be specified for an area of interest and vice versa. There are also a variety of specialty mesh features such as a mesh boundary layer available: adding finely spaced mesh layers along a boundary. How to use all of these tools effectively to mesh a geometry is why meshing can be one of the most challenging aspects of FEM modeling.

2.4.1 Meshing The VI Model

Now that we know a little about meshing in general, we can move on and mesh our VI model geometry. The first choice we need to make is which type of element to use, and in order to do that we need to think about the gradients of the dependent variables.

From van Genuchten's retention curves, we know there will be a large soil moisture gradient in the capillary zone, which will need a relatively fine mesh to be resolved. The airflow from Darcy's Law will forming some sort of arcing streamline from the ground surface to the foundation crack; the pressure gradient will be inline with these streamline. The concentration gradient is difficult to predict a priori, but there likely will be some gradient from the groundwater to the ground surface and foundation crack. Since many of these gradients intersect and go in different directions from each other it makes sense to use tetrahedral elements to mesh the geometry; these are the more general 3D elements.

Properly meshing our geometry can be a challenge due to the great range of geometric scale. The house and soil domains are on the order of meters while the foundation crack is only 1 cm side, and requires very fine meshing. This is not only due to its small size, but because the contaminant entry will be calculated based on the solution here, which largely determines the indoor contaminant concentration.

The COMSOL meshing algorithm only require a few parameters to relatively mesh a geometry with tetrahedrals. A description of each parameter and its value can be seen in Table 2.1.

Table 2.1: Inputs to COMSOLs meshing algorithm.

Input	Value	Description
Maximum element size	1.5 m	Maximum size of a element
Minimum element size	1 mm	Minimum size of a element
Maximum element growth rate	1.3	Maximum allowed size increase of adjacent elements. 1.3 indicates that an element can only be 30% larger than its neighbor. A smaller value gives a finer mesh.
Curvature factor	0.4	Ratio between the boundary element size and the geometry curvature radius. A smaller value gives a finer mesh.
Resolution of narrow regions	1	Control the number of layers of elements that are created in narrow regions. A larger value gives a finer mesh.

2.4.2 Boundary Layer Mesh

When posed with steep gradients in one particular direction at boundaries, as we are here, it is often useful to use a *boundary layer mesh* at the impacted boundaries. This is a type of mesh that introduces a dense layer of meshes along the normal direction from a boundary. The number of layers are supplied by the user, and in our case we will use 8 layers, but more could be added if needed. The distance

between each layer is determined by the size of the other elements in its vicinity, as well as the distance growth rate between each layer, which we set to 1.3, i.e. the distance increases by 30% for each layer. Figure 2.7 shows our completed mesh.

2.5 Solver Configuration

A solver(s) is required to solve the VI model, and a few considerations need to be taken when choosing one. For simplicity we will now first consider a stationary or steady-state problem. Since our model is a multiphysics problem, i.e. many of the physics depend on each other, we first need consider how to couple our physics. The physics can be coupled by either using a *segregated* or *fully coupled* approach.

Segregated vs. fully coupled physics In a segregated solver, each governing equation or physics is solved separately in a specific order. For instance, in our VI example we could solve Darcy's Law first, get some solution, then use that in the transport equation, solve that, and then solve the indoor concentration equation, i.e. we solve one system of equation per physics. These steps are simply iterated until convergence occurs in all of the separated steps. The fully coupled approach assembles a single large system of equation from all of the physics. Both of these approaches will reach the same solution, but the fully coupled approach will do so faster, but at the expense of using more memory.

Direct vs. iterative solver Within each of these coupling approaches, we need to specify a solver to solve the system of equations. Here we are again faced with a choice, and we could either use a *direct* or *iterative* solver. Direct solvers, as the name implies, arrive at a solution directly and are based on LU-decomposition. Iterative solvers on the other hand, iteratively approach the solution, and are based on conjugate gradient method. The advantage of direct solvers is that they are faster, but use more memory, while iterative solvers are slower but use less memory. In terms of choosing a solver algorithm, there are many options, but MUMPS and GMRES will be used as the respective algorithm for direct and iterative solvers.

Time-dependent solvers To solve a transient or time-dependent problem (which will be done in subsequent chapters) a solver to step forward in time is required. A too large time step will cause stability issues and ultimately convergence will be impossible, but obviously some discrete time step is required for a solution to be achievable. A time-dependent solver picks an appropriate time-step and there are some popular approaches, such as using some high-order Runge-Kutta (RK) or backwards differentiation formula (BDF). Regardless of the type of solver, for each time step the system of equations will be solved using one of the aforementioned solvers. The difference between RK and BDF is that RK explicitly discretizes time while BDF does so implicitly. In this work we will only use BDF as it is more stable than RK.

Choosing solvers The choice of solver will not affect (or should not at least) the solution to the problem. However, it can have a large impact on computational time and resources, and these considerations dictate solver choice (this is also partially

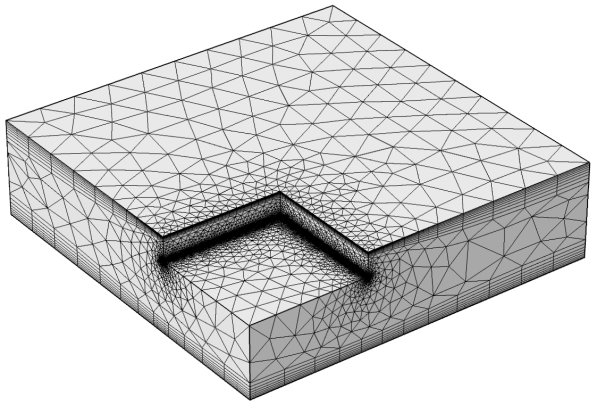

(a) The darker perimeter around the foundation highlights the higher mesh density along the foundation crack.

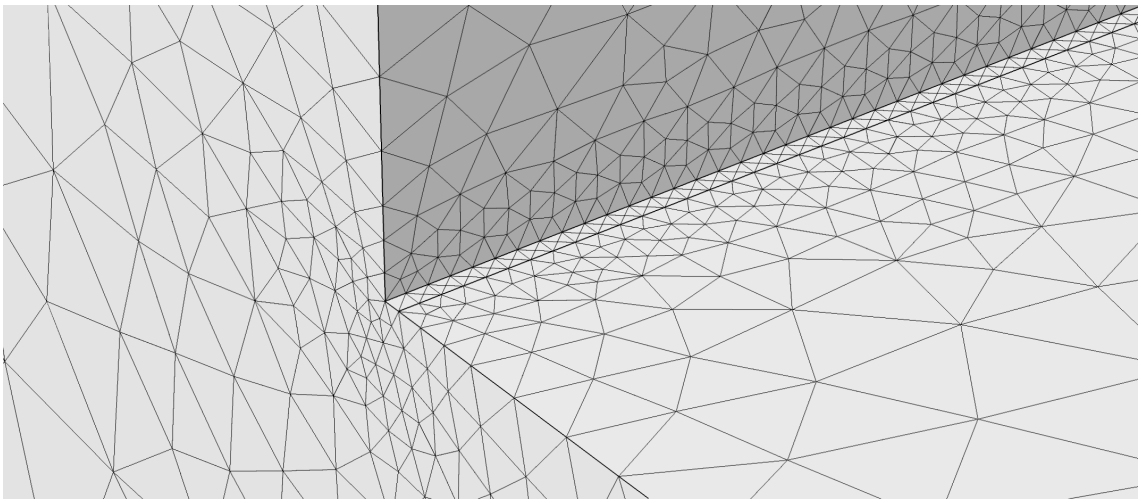

(b) Close-up of the foundation crack mesh.

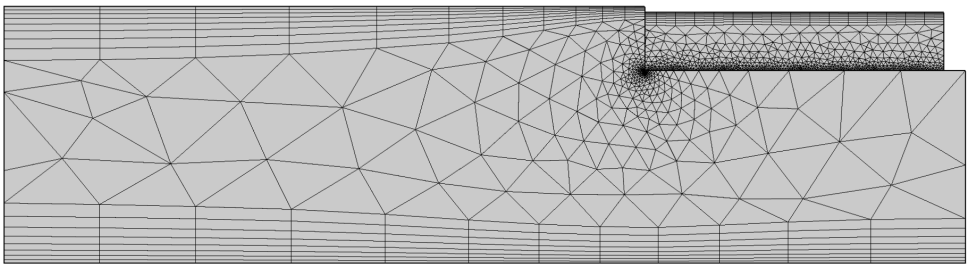

(c) Side-view highlighting the boundary layer mesh.

Figure 2.7: Initial mesh of our geometry.

dependent on the mesh used, as this will affect memory usage too). In this example, and throughout the models used in this work, we will favor speed over memory and

therefore fully couple all our equations and use direct solvers.

2.5.1 Adaptive Mesh Refinement

The accuracy of the solution obtained by FEM is dependent on the quality of the mesh, something that was discussed in section 2.4. While the mesh designer can do much to create a mesh that performs well for the particular problem posed, refinement of the mesh is often needed and should be performed for every new model.

There are two types of mesh refinements in FEM. The first type reduces the size of the elements and thereby the accuracy of the solution, this is called *h-type* refinement (h is often used to denote the mesh size). The second increases the order of the polynomial of the basis function, called *p-type* refinement which will likewise increases the solution accuracy.

h-type refinement is generally more attractive because it is simpler and the computational cost of p-type refinement increase faster than h-type. However, p-types are useful if the user imports an already existing mesh, and is unable to change it, rendering h-type refinement impossible. These two method can be combined to perform a *hp-type* refinement.

Refinement is usually done by an algorithm, which is possible because FEM has the built-in ability to estimate the local error of the solution anywhere in the domain. The downside with using an algorithm is that the user has little control over how the mesh is refined. The user can also manually refine the mesh by solving the model and plot how some relevant metric converges as the mesh is refined. This can be a very time consuming, and therefore algorithms are usually preferable; a hybrid solution is to manually alter the mesh after the algorithmic mesh refinement.

Refinement can either be done locally or globally. Global refinement involves defining some singular metric that will be used to evaluate the quality of the mesh, e.g. one might use the total stress in a metal bar as a metric here. In local refinement, one still has to define some metric for evaluating the quality of the refinement, but evaluation only occurs on a subset of the domain, e.g. the stress on just one boundary of the same metal bar. In both approaches the elements that have the largest estimated local error are refined; this error estimation is an inherent feature of FEM. The optimal type of refinement varies by problem, but a global refinement will generally be more computationally expensive.

In this work we will use a global h-type refinement and use the indoor contaminant concentration c_{in} as our refinement metric. COMSOLs refinement algorithm has the nice ability to reinitialize the mesh, and can thereby coarsen elements, i.e. increase h where the local error is very small. This is handy as a fine mesh is not needed far away from the foundation crack - saving computational resources. In this example we will tell the algorithm to refine the mesh three times, and stop if the total number of elements exceed 1 million, with a maximum coarsening factor of 3, and element growth rate of 1.7, i.e. the number of elements increase by roughly 70% each iteration.

The result of this refinement can be seen in Figure 2.8 where the original and refined mesh are juxtaposed. Notice how the mesh is now denser near the foundation, the boundary layers tighter (in particular near the groundwater boundary), and how the elements are larger in the periphery. The original and refined meshes has 362,657

and 1,065,743 elements respectively.

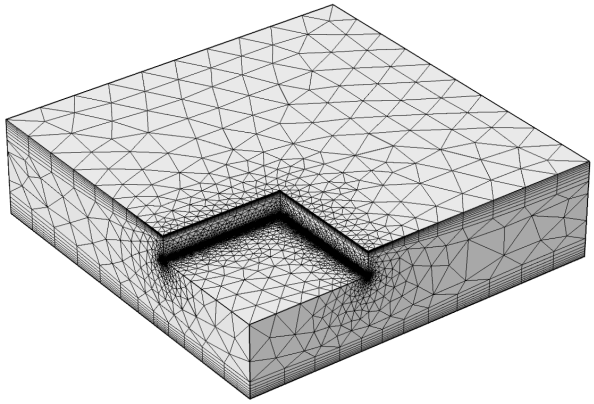

(a) Original mesh. 362,657 elements.

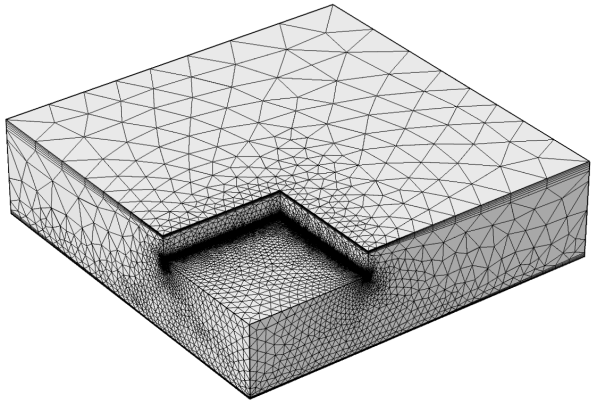

(b) Refined mesh after two steps of global refinement w.r.t. the indoor contaminant concentration. 1,065,743 elements.

Figure 2.8: Original and refined mesh.

2.6 Post-processing & Results

One of the benefits of using a FEM software like COMSOL is its advanced post-processing capabilities. This allows the user to examine the physics driving VI in great detail. Figure 2.9 shows the resulting pressure field from solving Darcy's Law, as well as the associated airflow streamlines in the soil. Here we see the pressure in the near foundation crack region is roughly the same as the house pressurization of $-5\,\mathrm{Pa}$, which quickly decreases towards the ground surface. It is also apparent how this pressure field induces a airflow from the ground surface, with air near the house heading relatively straight to the foundation crack, whereas the air further away from the house penetrates deeper into the soil and almost "whirlwinds" underneath the house.

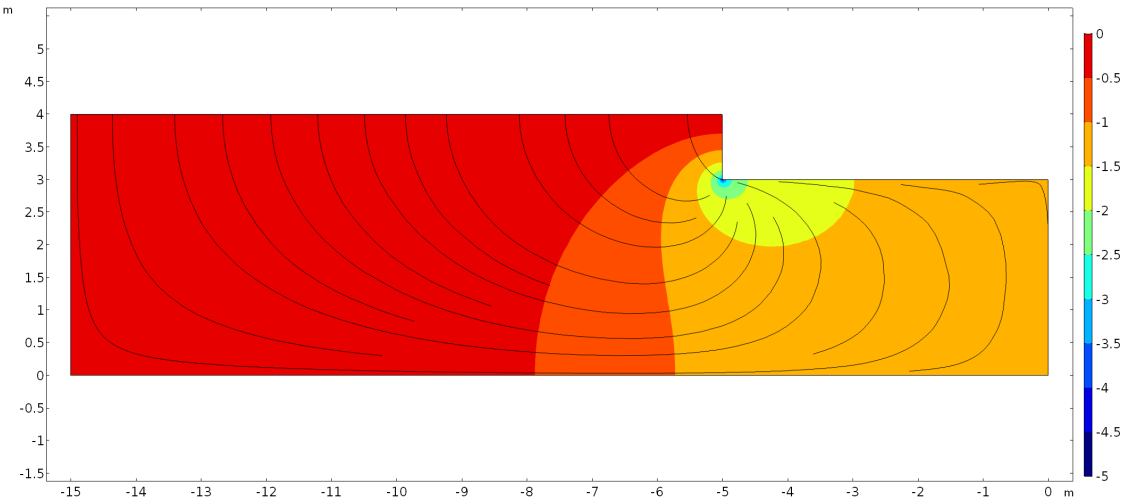

Figure 2.9: Pressure field from Darcy's Law with associated airflow streamlines.

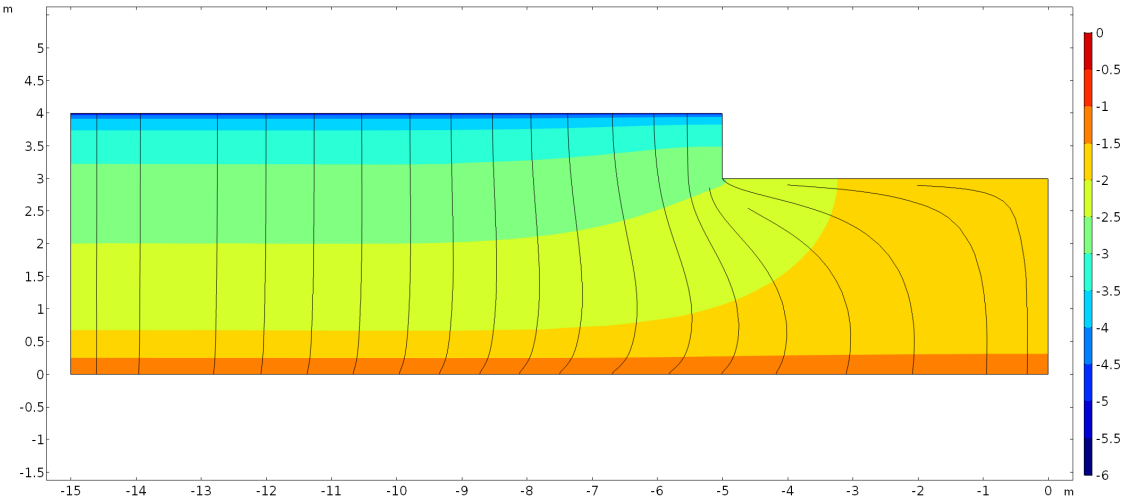

Figure 2.10: Contaminant concentration in the soil, normalized to groundwater concentration and log-transformed, with transport streamlines.

The contaminant concentration in the soil, normalized to the groundwater source concentration and log-transformed, with the contaminant flux streamlines, is examined in Figure 2.10. Here see that far away from the house, the contaminant vapor simply diffuse straight from the groundwater source to the atmosphere, while these accumulate underneath the house, which acts as a diffusion blocker. Bases on those streamlines we can conclude that the advective component of the flux is very here small. Perhaps surprisingly, we do not see a significant advective transport downwards along the wall of the house. However, considering the soil type is sandy loam, airflow velocities are expected to be small.

One might think that advective transport is large in the horizontal direction along the foundation slab, as the transport and airflow streamlines are so similar. However, by inspecting Figure 2.11 we see that airflow velocities are not great here than elsewhere, and therefore the advective transport is not either. To make sense of this, we can inspect the horizontal diffusive flux, divided by the magnitude of the

total flux

$$\frac{j_{\text{diff,y-direction}}}{|j_{\text{total}}|} \tag{2.40}$$

to see what portion of the total transport the diffusive horizontal make up here. The results of this is shown in Figure 2.12, where see that the horizontal diffusive flux in the left direction accounts for 80% of the total flux magnitude, as indicated by -0.8. This shows the power of modeling and how it can reveal things that at first seem intuitively correct, but in fact are not.

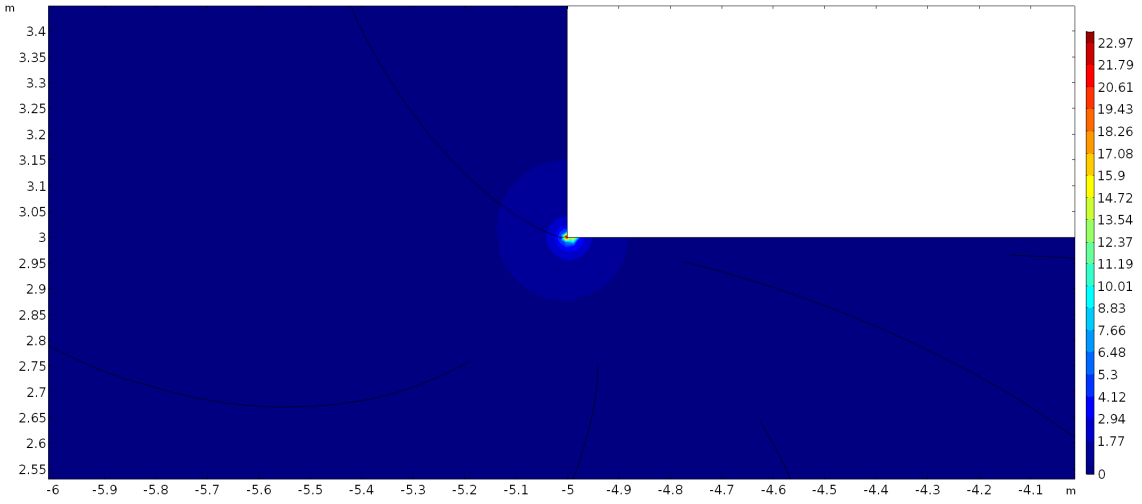

Figure 2.11: Airflow velocity [mm h^{-1}] near the foundation crack with associated its streamlines.

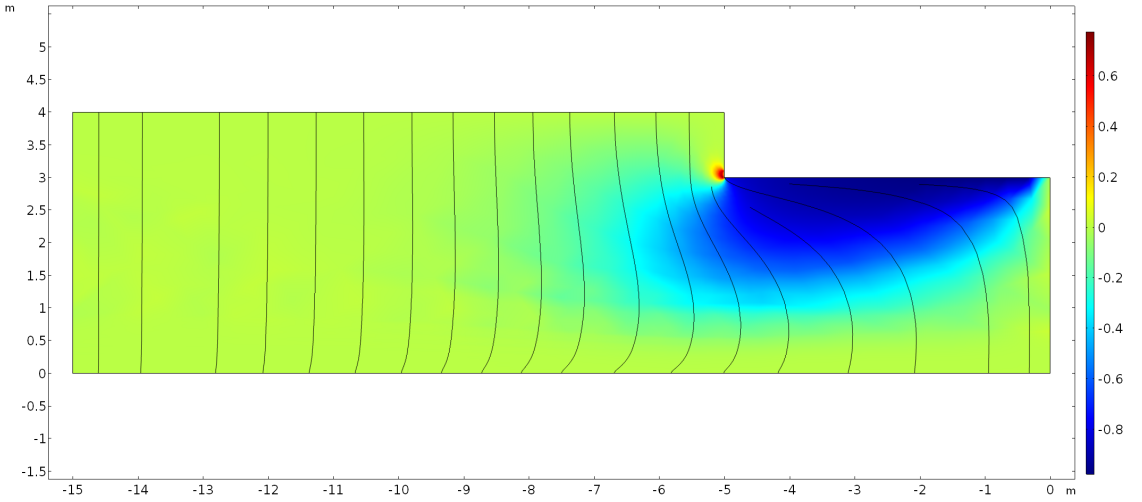

Figure 2.12: Horizontal diffusive flux component of the magnitude of the total flux. 1 here would indicates that all of the contaminant transport is due to diffusion, and occurs solely in the rightwards direction.

Another useful feature of post-processing is that it can be used for bug searching and to evaluate where the mesh can be potentially improved. The when numerically the transport equation used to model contaminant transport, there is a tendency for the solution to oscillate around the "true" solution, and thereby violate mass conservation, if the mesh size in a particular element is too large. This can be

quantified by the cell Péclet number, which characterizes the relative magnitude of advection/diffusion in a cell.

$$\mathrm{Pe}_{\mathrm{cell}} = \frac{\mathrm{adv}_{\mathrm{cell}}}{\mathrm{diff}_{\mathrm{cell}}} = \frac{u_g h}{2D_{\mathrm{eff}}} \tag{2.41}$$

here u_g [$\mathrm{m\,s^{-1}}$] is the soil-gas airflow velocity; h [m] is the mesh size in the element or cell; and D_{eff} [$\mathrm{m^2\,s^{-1}}$] is the effective diffusivity in the cell. If $\mathrm{Pe}_{\mathrm{cell}} > 1$ there is a risk that this oscillating behavior will manifest. Small exceedances, $\mathrm{Pe}_{\mathrm{cell}} < 25$, are usually able to be mitigated by various stabilization schemes, which are inherently integrated into COMSOL as well as many other FEM packages, but for larger values further mesh refinement may be required.

Figure 2.13 shows $\mathrm{Pe}_{\mathrm{cell}}$ as a volume plot, and excludes all values that fall below one. As we can see, only the region close to the groundwater exceeds $\mathrm{Pe}_{\mathrm{cell}}$, which is due to the very small D_{eff} there. The exceedance is small, so the stabilization scheme is able to compensate which is confirmed by Figure 2.10 (no oscillations visible). This is also a region where even if such oscillations occurred, would probably not affect the indoor contaminant concentration. Regardless, Figure 2.13 shows where the mesh may potentially be refined, which comes in handy to know if one runs a model where airflow velocities are significantly higher than in this example.

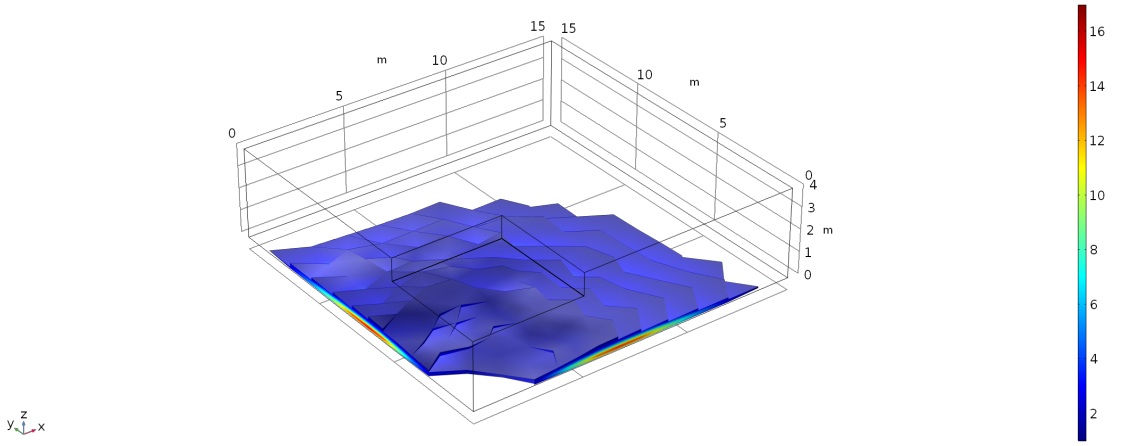

Figure 2.13: Volume plot showing where the cell Péclet number exceeds 1 and its actual value. I.e. it suggests where the mesh may be improved.

.1 Geometry Generation

To create our quarter geometry, only a few simple geometric objects and Boolean operations are required: two cuboids, two rectangles, one Boolean difference operation, and one Boolean join operation. Figure 2.3 shows the resulting geometry. Note that $z = 0\,\mathrm{m}$ is the groundwater/soil interface and the plane of symmetry is around the $(x, y) = (0\,\mathrm{m}, 0\,\mathrm{m})$ axis

To create the soil surrounding the building using the COMSOL geometry generator:

1. Create a 15 m by 15 m by 4 m block with its base at $(x, y, z) = (0\,\mathrm{m}, 0\,\mathrm{m}, 0\,\mathrm{m})$. This is the entire soil domain.

2. Create a 5 m by 5 m by 1 m block with its base at $(x, y, z) = (0\,\mathrm{m}, 0\,\mathrm{m}, 3\,\mathrm{m})$. This will represent the volume that the house take up in the soil, i.e. the underground portion of the basement.

3. Perform a difference operation, removing the "basement" block from the "soil" block.

At this point you will see that a quarter soil domain has been created, with an empty space that represents a house with a foundation slab located 1 m bgs.

The foundation crack will be modeled by joining two 1 cm wide strip that spans the perimeter of the surface that represents the house foundation. This strip is created by joining two rectangles on foundation surface:

1. Define a work plane 3 m above zero. This allows us to place two-dimensional objects on the surface of or inside a three-dimensional object.

2. On the work plane create a 5 m by 1 cm rectangle with its base at $(x, y) = (0\,\mathrm{m}, 5\,\mathrm{m} - 1\,\mathrm{cm})$. This represents one side of the perimeter crack.

3. Copy the rectangle and rotate it 90° around the corner of the foundation, i.e. $(x, y) = (5\,\mathrm{m} - 0.5\,\mathrm{cm}, 5\,\mathrm{m} - 0.5\,\mathrm{cm})$.

4. Join the two rectangles to create a unified perimeter foundation crack.

Now the geometry of this VI scenario is complete.

.2 Properties

Table 2: Properties and van Genuchten parameters of select soil types[**abreu˙conceptual˙2012**].

Soil type	Permeability κ (m^2)	Density ρ (kg/m^3)	Porosity θ_t	Residual moisture θ_r	van Genucht α
Sand	9.9×10^{-12}	1430	0.38	5.3×10^{-2}	3.5
Loamy sand	1.6×10^{-12}	1430	0.39	4.9×10^{-2}	3.5
Sandy loam	5.9×10^{-13}	1460	0.39	3.9×10^{-2}	2.7
Sandy clay loam	2.0×10^{-13}	1430	0.38	6.3×10^{-2}	2.1
Loam	1.9×10^{-13}	1380	0.40	6.1×10^{-2}	1.5
Silt loam	2.8×10^{-13}	1380	0.44	6.5×10^{-2}	0.51
Clay loam	1.3×10^{-13}	1500	0.44	7.9×10^{-2}	1.6
Silty clay loam	1.7×10^{-13}	1390	0.48	9.0×10^{-2}	0.84
Silty clay	1.5×10^{-13}	1300	0.48	1.1×10^{-1}	1.6
Silt	6.7×10^{-13}	1260	0.49	5.0×10^{-2}	0.66
Sandy clay	1.7×10^{-13}	1470	0.39	1.2×10^{-1}	3.3
Clay	2.3×10^{-13}	1330	0.46	9.8×10^{-2}	1.3
Gravel[**dan˙capillary˙2012**]	1.3×10^{-9}	1430	0.42	5.0×10^{-3}	100

Appendix A

Preferential Pathways: Drivers Of Temporal & Spatial Variability In Vapor Intrusion

Abstract

Vapor intrusion (VI) investigations, the effort to determine the exposure and associated human health-risk at a VI impacted building, are often complicated by significant spatial and temporal variability in concentrations of contaminants of concern. Over the years there have been efforts to develop new techniques and methodologies that aim to reduce the uncertainties associated with these variabilities. The goal is to simplify and improve the robustness of VI site investigations. The development of the controlled pressure method (CPM), where the pressurization of a building is controlled in an effort to increase or decrease contaminant entry into the building, is one such example. Another approach is to use indicators, tracers, and surrogates (ITS) to help guide when to conduct site investigations, ideally increasing the likelihood of determining the maximum indoor contaminant concentrations.

Both of these approaches rely on a quasi-deterministic relationship between some external variable, such as building pressurization, and indoor contaminant concentration. However, site-specific conditions can give rise to very different responses to such an external variable. To effectively use CPM or ITS, a better mechanistic understanding of contaminant transport and exposure is needed.

In this thesis, we develop three-dimensional finite element models of VI impacted buildings from a first principles perspective. These models combined with analysis of field data from VI sites, allows us to explore the physical mechanisms that drive VI. By considering the dominant contaminant transport mechanism at a site, e.g. if advective or diffusive transport dominates, we can explain why a change in building pressurization can lead to differences in contaminant concentration variability at different sites. We can also better understand how the various factors governing VI contribute to the overall variability.

By classifying the dominant contaminant transport mechanism at a site, we can more effectively anticipate how a particular site will respond to some external stimuli. This will in turn reduce the effort required to, and increase the robustness of the techniques used determine the relevant human exposure at a VI site.

A.1 Introduction

Long term vapor intrusion (VI) studies in both residential and larger commercial structures have raised concerns regarding significant observed transient behavior in indoor air contaminant concentrations[**u.s.˙environmental˙protection˙agency˙oswer˙2015**, **folkes˙observed˙2009**, **holton˙temporal˙2013**, **johnston˙spatiotemporal˙2014**, **hosangadi˙high-frequency˙2017**, **mchugh˙recent˙2017**, **u.s.˙environmental˙protection˙ag** a phenomena that has previously been observed at houses impacted by radon intrusion[**hubbard˙t** Such variations make it difficult for those charged with protecting human health to formulate a response and appropriate risk evaluation. Furthermore there is uncertainty within the VI community regarding how to best develop sampling strategies to address this problem[**u.s.˙environmental˙protection˙agency˙oswer˙2015**, **holton˙temporal˙** **johnson˙integrated˙2016**, **mchugh˙recent˙2017**].

To address these concerns, the EPA purchased two VI impacted houses and outfitted them with a wide variety of sensors and sampling instrumentation to study VI at these houses in great detail. Indoor contaminant concentration as well soil-gas and groundwater contaminant concentration at different depths and locations were recorded, while simultaneously recording metrics such as indoor and outdoor temperature, wind speed and direction, and building pressurization. These measurements were taken continuously over multiple years an unprecedented detailed dataset for exploring VI.

One of these houses was in Layton, Utah, near Hill AFB, and was purchased in collaboration with a research group at Arizona State University (ASU), who conducted most of the research at the site - this site will be referred to as the "ASU house" throughout this work[**holton˙temporal˙2013**]. The other was in duplex in Indianapolis, Indiana, and will be referred to as the "EPA duplex". There work was not primarily isolated to one group.

One thing both of these sites had in common was that after a few years of study, preferential pathways were discovered at the sites. A preferential pathway is typically thought of as some conduit that can transport large amounts of contaminant vapors into a building, in contrast with the slower vapor transport in soils.

At the ASU house, this took the form of a land drain underneath the house foundation, presumably to drain excess water from the sub-slab region. This land drain was connected to the nearby sewer and exited into a gravel layer under the foundation, near a breach in the slab. The sewer was buried deep enough to be partially submerged in the TCE contaminated groundwater, which likely infiltrated into the sewer. The land drain was later excavated and fitted with a valve, allowing the researchers to control its influence - which was revealed to be very significant[**guo˙identification˙2015**]. The details of this is covered further down.

At the EPA duplex, the sewer acted as a preferential pathway, somewhat similar to the ASU house, but the nature of this preferential pathway was quite different from the one at the ASU house. A tracer gas test demonstrated that contaminant vapors were directly transported into the duplex[**mchugh˙evidence˙2017**]; similar to a site in Boston, Massachusetts, where PCE was transported into a bathroom through broken plumbing fixtures[**pennell˙sewer˙2013**]. It was also demonstrated that contaminated groundwater infiltrated the sewer a few blocks away from the duplex, where a dry-cleaners had previously been. This type of distributed contamination via a sewer network has likewise been recorded in Denmark[**nielsen˙remediation˙2017**]

as a VI source - giving rise to a very different situation compared to radon intrusion.

It is also likely that the sewer pipe at the duplex leaked contaminant vapors somewhere near the vicinity of the house. This would give a situation that is similar to the ASU house land drain, but somewhat mitigated since the pipe leakiness is likely due to structural degradation, e.g. cracks in the mantle area; quite different from open channel flow from the ASU house land drain.

These works shows some of the diverse ways that a preferential pathway can play a role in VI, and our poor understanding in evaluating their significance. However, since the influence of the preferential pathway at the ASU house was able to be turned on and off (via the valve), we have an unprecedented opportunity to explore the effects of such a preferential pathway at a VI site.

A.1.1 The ASU House

The VI study at the ASU house had primarily two purposes:

1. Investigate VI with a particular focus on understanding the temporal and spatial variability.

2. Test and evaluate the performance of the controlled pressure method (CPM).

This was to be achieved by monitoring various metrics relevant to VI, such as building pressurization, air exchange rate, indoor and outdoor temperature, and other metrological variables, while simultaneously monitoring the indoor air contaminant concentration. Additionally, soil-gas and groundwater contaminant concentration underneath and around the house were monitored; the specific sampling locations, as well as a photo of the house, can be seen in Figure A.1. The study of the ASU house is one of the most detailed studies of a VI site to date and fully describing the experimental setup and measured metrics is beyond the scope of this work but is detailed in **holton˙temporal˙2013**[**holton˙temporal˙2013**].

CPM seeks to control the pressurization of the building, and thereby controlling the contaminant entry rate. In this framework, overpressurizing a building will eliminate contaminant entry rate into the building, thereby identifying indoor contaminant sources. By contrast, depressurizing a building will increase contaminant entry rate, giving a theoretical "worst-case" VI scenario. Here the researchers would use a 20 inch window box fan to control the pressurization of the building.

The site was monitored for roughly 1.5 years before the testing of the CPM system commenced. During this time, it was established that the indoor contaminant concentration fluctuated significantly at the site - roughly an order of magnitude on a weekly basis, while up to three or more orders of magnitude on a seasonal basis. Once the house was depressurized using the CPM system, indoor contaminant concentration increased to higher concentration levels previously recorded - an initial verification of the CPM framework[**holton˙long-term˙2015**].

However, during the CPM testing period, the researchers noticed that the house and nearby sewer seemingly communicated with each other. This was shown by the movement of a plastic tarp, which covered a nearby manhole, as the door of the house was opened and closed. This lead to the discovery of the land drain preferential pathway at the site; the location of it in relation to the house floorplan can be seen in Figure A.2 The land drain determined to exit into the gravel sublayer beneath

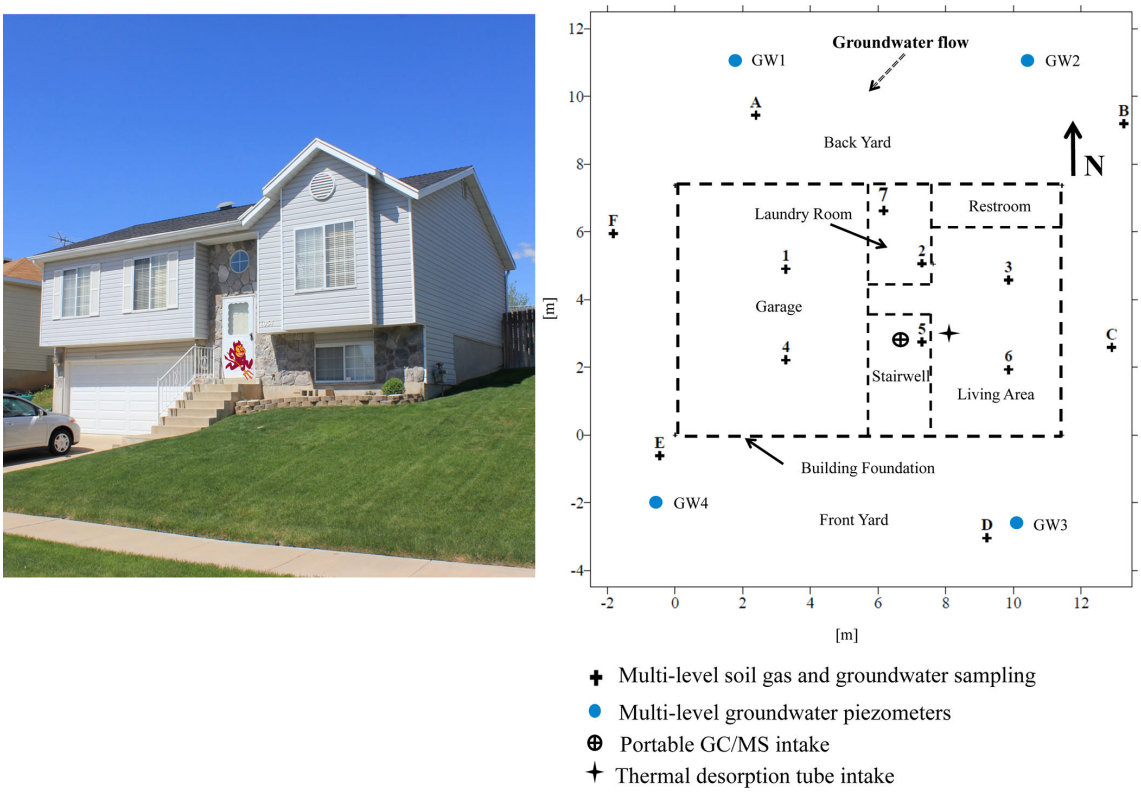

Figure A.1: Picture of the "ASU house" with floorplan showing the location of all subsurface sampling ports. Figure is from **holton˙temporal˙2013**[**holton˙temporal˙2013**]

the foundation, near a visible breach in the foundation slab, and was subsequently excavated and fitted with a butterfly valve [**guo˙identification˙2015**] to control its influence.

The land drain was closed towards the later part of the CPM study, which lead to a significant decrease in indoor contaminant concentration. This effect can be seen in Figure A.3, which shows the log-10 transformed indoor contaminant concentration for the entire study duration. Here the pre- and post-CPM periods are marked by colors, and the closing of the land drain by the black vertical line. Notice how the temporal variability in indoor contaminant concentration decrease significantly after the closing of the land drain.

Figure A.4 shows the same data, i.e. the log-10 transformed indoor contaminant concentration, but as a boxplot instead of a timeseries plot. Here the colored box represents the interquartile range (IQR) of the distribution - the middle line is the 50^{th} or median value, while the top and bottom of the represent the 75^{th} and 25^{th} percentile values. The whiskers are the extent of the dataset, while "outlier" points are given by the dots, here formally defined as data lying 1.5 times outside the IQR; these are "real" data points but simply plotted as outliers not to skew the IQR. This figure again reinforces the significant effect that the land drain preferential pathway had on the temporal indoor contaminant concentration variability at the ASU house.

In the VI field, it is widely held that the building pressurization relative to the ambient outdoor is a key driver of contaminant entry into VI impacted building. Since building pressurization fluctuations can occurs rapidly, this is a prime factor

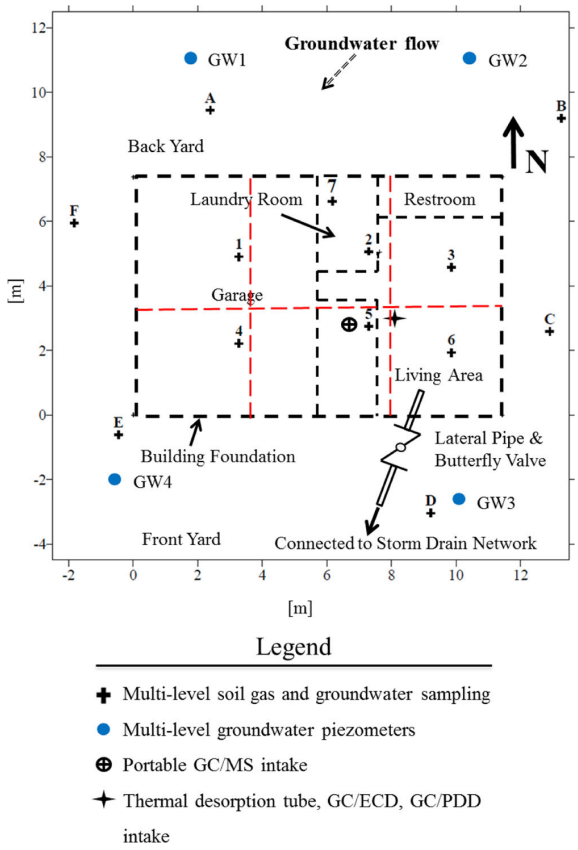

Figure A.2: Location of the land drain preferential pathway at the ASU house site. Figure is from **guo˙identification˙2015**[**guo˙identification˙2015**].

for investigating the transport dynamics of the preferential pathway. Figure A.5 considers the relationship between the indoor air concentration and building pressurization, specifically indoor/outdoor pressure difference, for the periods when the preferential pathway was open and closed. This clearly shows the dramatic change in sensitivity of the indoor contaminant concentration to building pressurization after the closing of the preferential pathway, which is not only apparent from visual inspect but from the change in the Pearson's r values for the considered periods. Pearson's r essentially tells us how linear correlation between two datasets; a value of 1 indicates that there is a perfect positive linear relationship, and -1 a perfectly negative linear relation. In our context, a negative value indicate that a decrease in building pressurization leads to an increase in indoor contaminant concentration, which makes sense as contaminant entry rates into the house would increase as it is further depressurized.

The question then becomes why this fundamental shift in the relationship between building pressurization and indoor contaminant concentration occurred, and how it relates to temporal variability in indoor contaminant concentration. Answering this is one of the primary objectives of this chapter, which will be done by developing a numerical model of a VI site that is *similar* to the ASU house, and in combination with comparison to the field data, will give insights how a preferential pathway can fundamentally alters contaminant transport at a VI site. We will also explore how such a preferential pathway can significantly contribute to the spatial variability contaminant concentration, in particular in the near sub-surface region.

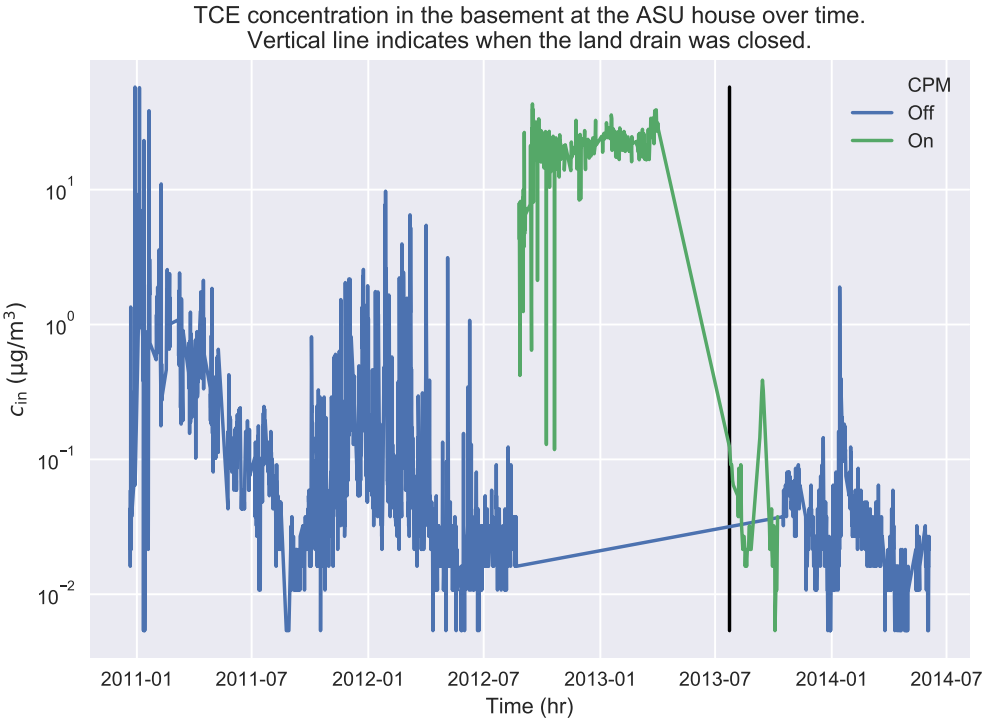

Figure A.3: The temporal variability of indoor air contaminant concentrations recorded at the ASU house. Measurements were taken in the basement. The periods were the CPM system was on and off are marked.

A.1.2 EPA Duplex

The EPA duplex was, similarly to the ASU house, a highly detailed VI study. Here the indoor contaminant concentrations of TCE, PCE, chloroform, and radon were measured in different floors of each side of the duplex, as well as in different locations and depths in the subsurface and groundwater - these sampling location ports, as well as a floorplan of the duplex can be seen in Figure A.6. These sampling ports also allowed pressure differences between different locations to be measured. Metrological data was collected throughout the study period, which lasted for around 2.5 years, and included indoor and outdoor temperatures, wind speed and direction, precipitation, and recorded snow coverage[**u.s.˙environmental˙protection˙agency˙assessment˙2015**].

The was likewise characterized by significant temporal variability in indoor contaminant concentrations, which can be seen in Figure A.7. This variability was not as significant as was recorded at the ASU house, but substantial nonetheless. Understanding the observed variability was a major focus of this study, but additionally the researchers sought to evaluate the efficacy of a subslab depressurization (SSD) system. A SSD system depressurizes the subslab region, which diverts contaminant vapors from entering the structure into a pipe placed through the foundation slab, which then are expelled into the atmosphere[**u.s.˙environmental˙protection˙agency˙assessme**
There are many different possible configurations of these pipes, and their design is its own research topic, one which will not be addressed in this work. However, it is useful to know, and we will only consider data before the implementation of the SSD system. It should also be noted that only one side of the duplex was heated,

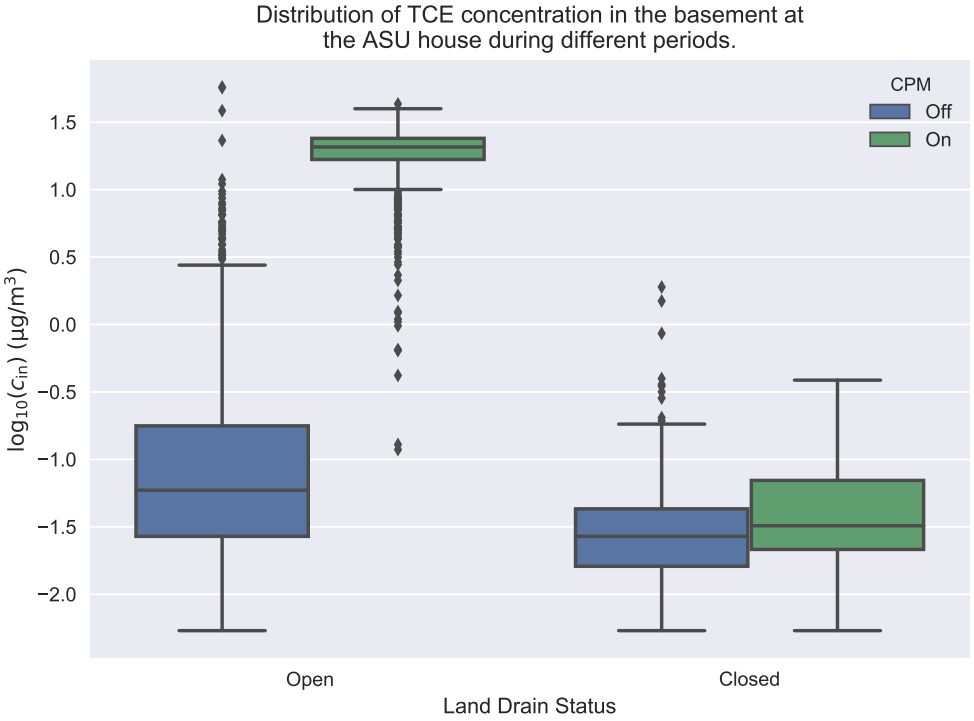

Figure A.4: Boxplot showing the log-10 transformed TCE concentrations at the ASU house. The CPM and natural periods, and the period before and after the land drain was closed are considered separately. The box signifies the interquartile range (IQR) of values, with the central line representing the median value, and the top and bottom of the box are the 25th and 75th percentiles. The whiskers extend to 1.5 times the IQR. Markers indicate outlier data points that fall outside the whiskers.

and we will only consider data from this side.

Like the ASU house, it was later determined that a sewer preferential pathway existed at the site. This preferential pathway seemingly played a very different role than the one found at the ASU house, and different in primarily two ways:

1. Infiltration of contaminant vapors did not occur near the duplex, but instead occurred a few blocks away - at the site of an old dry cleaner.

2. Communication between this preferential pathway and the indoor environment does not seem to have been as strong; the researchers believe that this may be due to the poor condition of the sewer pipe, which may have leaked somewhere along its path.

The first of these points was demonstrated by **mchugh˙evidence˙2017**[**mchugh˙evidence˙2017**], which tracked contaminant vapors along the length of the sewer system. The second point, or rather the evidence that communication between the indoor environment and the preferential pathway may not have been so strong is indicated by the lower temporal indoor contaminant concentration variability. It is also indicated by the weaker association between indoor contaminant concentration and the indoor/outdoor pressure difference, which can be seen in Figure A.8; this weaker

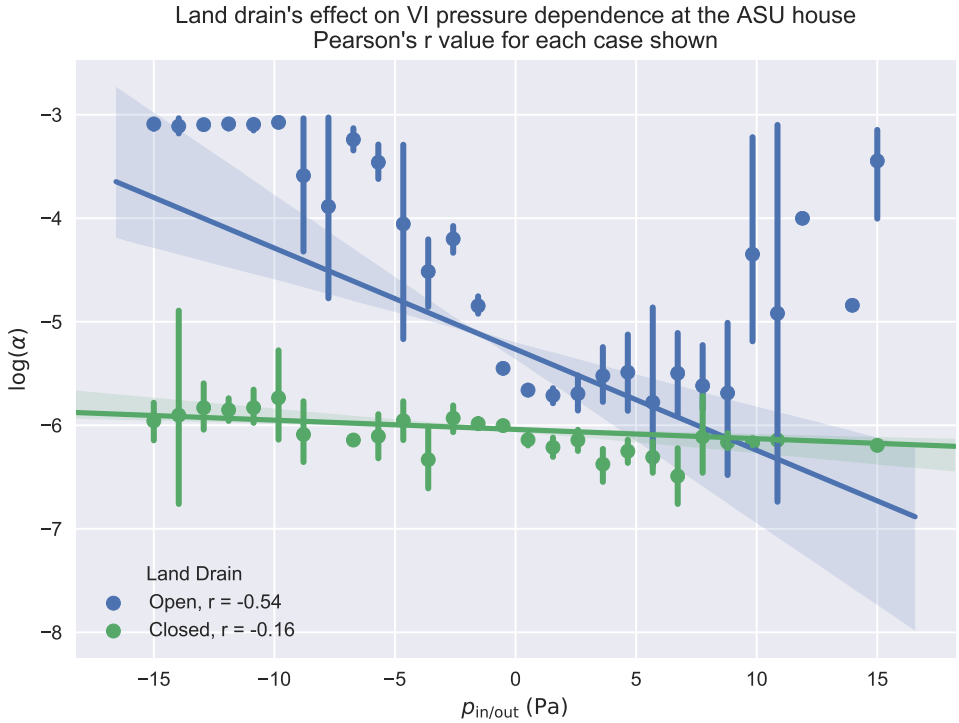

Figure A.5: Regression plot showing the indoor/outdoor pressure difference dependence on indoor air concentration. Here the indoor air concentration is normalized to the groundwater source concentration, i.e. attenuation factor, and log-10 transformed. Data is placed in evenly spaced (but not sized) bins. The bars indicate the 95% confidence intervals.

association is indicated by the smaller Pearson's r values compared to the ones at the ASU house before he closing of that preferential pathway.

Unfortunately, the EPA duplex preferential pathway is less well characterized, and its influence was never removed. This makes it difficult to assess how it contributed to overall VI at the site, or the observed temporal variability in indoor contaminant concentrations. However, it is possible to explore if the preferential pathway leaked somewhere near the site - which likewise will be a focus in this chapter.

Determining leakiness of the preferential pathway will be done by performing a kriging analysis of the measured soil-gas contaminant concentrations. Kriging is a type of interpolation technique which allows sparse data to be interpolated in multiple dimensions; ideal for interpolating soil-gas contaminant concentration in the soil surrounding the duplex. This way we can visually inspect the interpolated soil-gas contaminant concentration for "hot spots", which could indicate where such a leak might be.

A.2 Preferential Pathway Model

To investigate the role a land drain type preferential pathway may have on a VI site, we extend the VI model presented in Chapter **??**. By adding a gravel sub-base

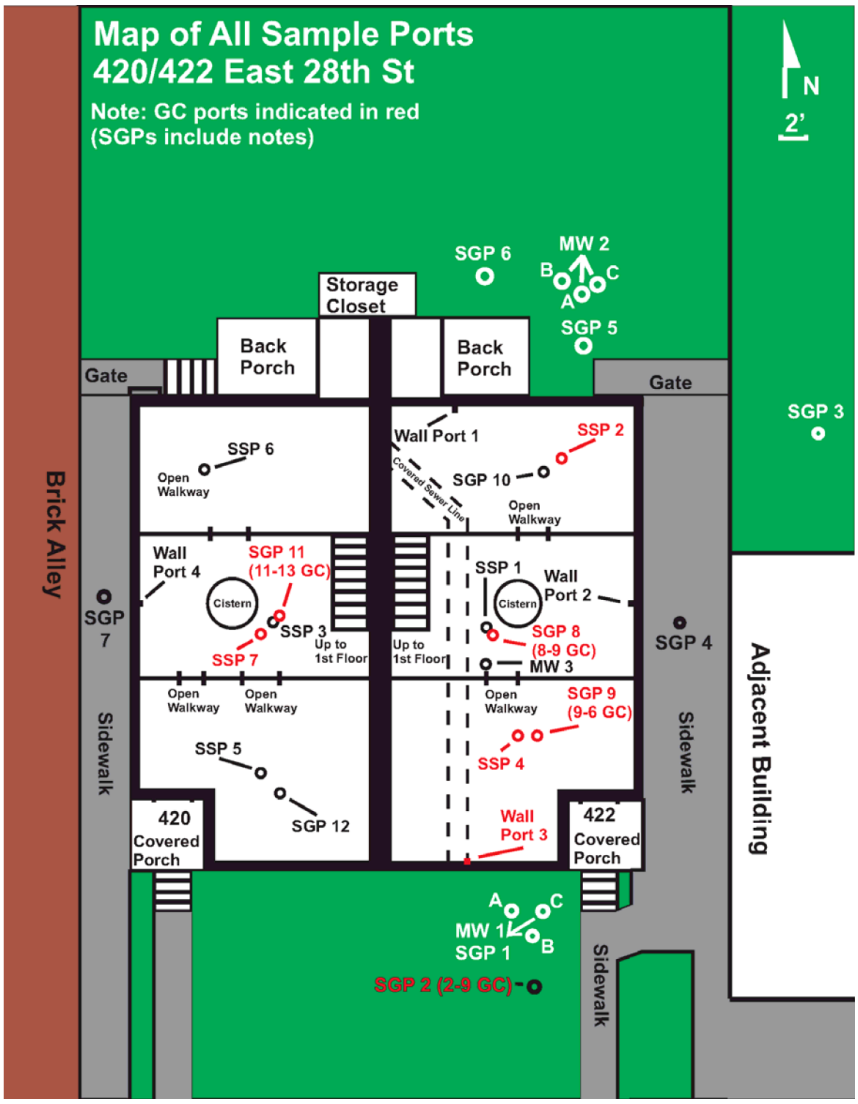

Figure A.6: Birdseye view of the EPA duplex, listing all the sampling location ports.

layer underneath the foundation slab and a preferential pathway to this model, we end up with a VI scenario that is similar to the ASU house.

Here we assume the gravel sub-base layer is 30 cm thick and extends from the edges of the foundation slab. While the exact thickness of the gravel sub-base layer at the ASU house is not known, it was estimated to be roughly that thick, and is not an uncommon thickness in many constructions. The gravel sub-base, unlike the rest of the soil, is going to be relatively dry; it is covered by the foundation slab, so no rain infiltration will occur and due to the coarseness of the gravel, no moisture will be drawn up by capillary force. Nonetheless, some van Genuchten parameters for the gravel are necessary to solve the model. Additionally, based on the site description, we will assume that the surrounding soil is sandy clay, a choice likewise made by **guo˙vapor˙2015**[**guo˙vapor˙2015**], one of the researchers at the ASU house. Table 2 has the van Genuchten parameters used to model these.

Based on the description of the land drain preferential pathway at the ASU site, we will model a preferential pathway as 10 cm diameter pipe that exits at the interface between the soil and gravel sub-base layer; placing it near the foundation crack - similar to the ASU house[**guo˙identification˙2015**]. To model the physi-

cal implications of the preferential pathway, we need to supply the model with two boundary conditions - one to solve Darcy's Law, and another to solve the contaminant transport governing equation. Figure A.9 shows the described scenario.

Since the preferential pathway is an open pipe, resistance to flow through it will be very small compared to the soil. Thus, the ground surface and the pipe are both sources of air to the soil domain and both are assumed to exist at reference atmospheric pressure.

$$\frac{\partial}{\partial t}(\rho\theta_g) + \nabla \cdot \rho\Big(- \frac{(1-k_r)\kappa}{\mu}\nabla p\Big) = 0 \tag{A.1}$$

Ground surface $p = 0\,\mathrm{Pa}$ (A.2)

Preferential pathway $p = 0\,\mathrm{Pa}$ (A.3)

Foundation crack $p = p_{\mathrm{in/out}}\,\mathrm{Pa}$ (A.4)

Remaining $-\vec{n} \cdot \rho\vec{u} = 0$ (A.5)

$p_{\mathrm{in/out}}$ is not specified here as we will parametrically choose values here.

The air in the pipe is also assumed to be contaminated with TCE at a vapor concentration equal to the vapor in equilibrium with the groundwater contaminant concentration below the structure. This assumption is based on contaminant samples taken from a manhole near the ASU house[**guo˙vapor˙2015**].

$$(\theta_w + \theta_g K_H)\frac{\partial c_w}{\partial t} = \nabla \cdot (D_{\mathrm{eff}}\nabla c_w) - K_H\vec{u}_g \cdot \nabla c_w \tag{A.6}$$

Atmosphere $c_w = 0\,\mathrm{mol\,m^{-3}}$ (A.7)

Groundwater $c_w = c_{gw}\,\mathrm{mol\,m^{-3}}$ (A.8)

Preferential pathway $c_g = c_{gw}K_H\,\mathrm{mol\,m^{-3}}$ (A.9)

Foundation crack $-\vec{n} \cdot \vec{N} = \dfrac{-j_{ck}}{K_H}\,\mathrm{mol\,m^{-2}\,s^{-1}}$ (A.10)

All other $-\vec{n} \cdot \vec{N} = 0\,\mathrm{mol\,m^{-2}\,s^{-1}}$ (A.11)

Note that we still neglecting any sorption in the soil. We will likewise normalize all concentrations to the source concentration c_{gw}, and as such the value of it does not matter.

The preferential pathway at the ASU house was connected to the nearby sewer and thereby the pipe ran between it and its exit in the gravel sub-base layer. Explicitly modeling the preferential pathway in our model would requires a significant number of elements and at little gain; contaminant vapor transport in the far corners of the model are not of great interest. To save computational resources only the exit of the pipe is modeled as a 10 cm diameter circle. This is especially important when we consider that pipe only allows for one plane of symmetry instead of two, and half of the model geometry has to be explicitly constructed instead of just a quarter like in Chapter **??**. Figure A.10 shows the resulting meshed geometry.

contrasting

A.3 Temporal Variability & Preferential Pathways

In the calculation results shown in Figure A.11, a preferential pathway is assumed to provide air containing contaminant vapor at a concentration equivalent to the vapor in equilibrium with the underlying groundwater source. Here, the indoor air exchange rate A_e was assumed to be a constant 0.5 per hour, and $p_{\text{in/out}}$ was varied from -5 to 5 Pa. Values of predicted indoor air contaminant concentrations, c_{in} were obtained from steady state calculations. The predicted c_{in} values were then normalized by the assumed vapor concentration in equilibrium with groundwater c_{gw}, giving the attenuation from groundwater α_{gw}. The predicted values of α_{gw} as a function of $p_{\text{in/out}}$ are given by the solid line Figure A.11. These predicted values are compared to actual measured α_{gw} values from the ASU House for the period during which the preferential pathway was open given by the blue points.

The model successfully predicts the observed trends in α_{gw} as $p_{\text{in/out}}$ decreases (increased depressurization) but somewhat underpredicts α_{gw} as the house is over-pressurized. Most significantly, the model captures that even for a small increase in depressurization (0 to -5 Pa) a very large increase in α_{gw} (two order of magnitude) can occur.

The model is also able to capture the weak trend in α_{gw} with $p_{\text{in/out}}$ when a preferential pathway is absent, but when there still exists a permeable subslab region. These results given by the green line in Figure A.11. These results are again in agreement with what was observed at the ASU House when the preferential pathway was closed, i.e. that there was a much more modest variation in indoor air concentration, irrespective of pressure, when the preferential pathway was cut off.

This shows the significant contribution that such a preferential pathway may have at a VI site. First, the preferential pathway acts not only as a source of contaminant vapor, but also as a source of air to the subslab. Because of the large resistance to soil gas flow in the surrounding soil, having a local source of air to support the increase of advective flow into the structure from the subslab region makes a large difference.

While there obviously is still some variability unaccounted for, as indicated by the error bars in Figure A.11, we can say with some confidence that the model is able to capture the general influence of such a preferential pathway. This opens us up to explore some of the factors that may be crucial for such an influence. Using our model, we rerun some of the scenarios, but this time consider two more cases:

1. We remove the gravel sub-base layer but keep the preferential pathway.

2. We keep the gravel sub-base layer, but remove contaminant vapor from the preferential pathway, i.e. it contains "clean" air.

The results of running these cases can be seen in Figure A.12.

Here the original modeling results and associated data from the period before the closing of the preferential pathway is again given by blue The case corresponding to the removal of contaminant vapors from the preferential pathway case is given by the green line, while the removal of the gravel sub-base care is given by red.

The removal of contaminant vapors from the preferential pathway largely eliminates the significant increase of α_{gw} with respect to p_{in} as given by blue in Figure A.11. However, the increase is larger than when the preferential pathway was absent

as indicated by green in Figure A.11. This shows that a preferential pathway similar to the one found at the ASU house does two things.

First, it provides a preferential source of air, and the depressurized building is able to much easier draw air from the preferential pathway than the surrounding soil; the soil offers a huge resistance to airflow and thus advective transport. Second, the increase in "advective potential" is inadequate to cause the same sort of effect as observed at the ASU house, and a preferential source of contaminant vapors is also required - two conditions that were seemingly fulfilled at the ASU house.

The removal of the gravel sub-base likewise also has a significant effect on the modeling results, and without it the full potential of a preferential pathway is seemingly unrealized. This can again be understood by understanding the significant resistance to contaminant transport that soils can present. This adds a third condition for such a preferential pathways influence - a medium for effective communication between the preferential pathway and indoor environment is necessary.

This can be shown by analyzing the Péclet number for transport through the foundation crack. The Péclet number is a dimensionless number defined as the ratio between advective and diffusive transport across some characteristic length, i.e. it tell us if transport is advective or diffusion dominated. For transport through the foundation crack we define this as

$$\mathrm{Pe} = \frac{\text{advection}}{\text{diffusion}} = \frac{u_{\mathrm{ck}} L_{\mathrm{slab}}}{D_{\mathrm{g}}} \tag{A.12}$$

here u_{ck} $[\mathrm{m\,s^{-1}}]$ is the airflow velocity across through the crackl $L_{\mathrm{slab}} = 15\,\mathrm{cm}$ is the thickness of the foundation slab, i.e. the characteristic length; and $D_g = 6.87 \times 10^{-6}\,\mathrm{m^2\,s^{-1}}$ is the diffusivity of TCE in pure air.

The value of Pe charcterizes transport as such:

$\mathrm{Pe} \gg 1$	Advection dominated
$\mathrm{Pe} \ll 1$	Diffusion dominated
$\mathrm{Pe} = 1$	Advection and diffusion equal

Figure A.13 shows the Péclet number for three of the modeled cases:

1. Preferential pathway and gravel sub-base layer present
2. Preferential pathway present but gravel sub-base layer absent
3. Preferential pathway absent but gravel sub-base layer present

Note that the cases when $p_{\mathrm{in}} > 0\,\mathrm{Pa}$ are not plotted, as the only different is the sign of the Péclet number - by our definition $u_{\mathrm{ck}} > 0$ indicates airflow into the house. This figure shows that it is only through the combination of a preferential pathway and a gravel sub-base layer that advective transport is able to dominate; diffusive transport dominates for the other cases which explains the weak correlation between α_{gw} and p_{in} in Figure A.12 when the preferential pathway was removed. Likewise it explains the dramatic increase of α_{gw} as p_{in} decreases when the gravel sub-base and preferential pathway were present, as advective transport only starts to dominate after $p_{\mathrm{in}} < -2.5\,\mathrm{Pa}$.

To summarize, for a preferential pathway to have a significant influence at a VI site, the following conditions need to be fulfilled:

1. A preferential source of air in required to enhance the advective transport potential at the site.

2. Contaminant vapors must likewise be preferentially supplied.

3. There needs to exist a medium to facilitate effective communication between the preferential pathway and the indoor environment.

While this may seem like some specific conditions to be fulfilled for a preferential pathway to be so impactful, it can easily be generalized to other scenarios. For instance, one could easily imagine a situation where a house has a gravel backfill surrounding it, with some other subsurface source - like a leaky sewer pipe (that does not exit anywhere the building). Under such a circumstance, one could conceivably observe a similar effect in the indoor contaminant concentration caused by a very different scenario.

A.3.1 Role Of Air Exchange Rate

Simulations so far has assumed that air exchange rate is at a constant $0.5\,\mathrm{h}^{-1}$ irrespective of the house pressurization. This is not quite realistic, as air exchange rates are constantly fluctuating, and this will have an impact on indoor contaminant concentrations. To account for this, we will again rerun our model simulations, but this time assuming different air exchange rate values, and if this can capture some more of the observed variability.

Ideally, we would wish to be able to determine air exchange rate based on site conditions, and in particular building pressurization. Determining air exchange rate exactly is difficult, and is influenced by building pressurization, indoor/outdoor temperature differences, wind, operation of HVAC systems, etc. This is a topic that will be expanded on in Chapter (TBD).

Air exchange rates are usually legally regulated as part of local building ordinances, and depending on the type of building, its values and bounds are usually more or less known. Instead, we will rerun the model and assume a wider range of constant air exchange rate values. At the ASU house, air exchange rates were measured using a tracer-gas study, and the the 10th, 50th, and 90th percentile air exchange rate values, as well as the corresponding values from the EPA duplex, and an independent EPA study that measured air exchange rates nationwide in the USA, all of which can be seen in Table A.1. Based on this we will rerun the model using air exchange values of 0.1, 0.5, and $0.9\,\mathrm{h}^{-1}$.

	Percentile		
	10th	50th	9
EPA study[**u.s.˙epa˙exposure˙2011**, **m.˙d.˙koontz˙estimation˙1995**]	0.16-0.2	0.35-0.49	1.21
ASU house[**holton˙temporal˙2013**, **guo˙identification˙2015**]	0.21	0.43	0
EPA duplex[**u.s.˙environmental˙protection˙agency˙assessment˙2015**]	0.34	0.74	1

Table A.1: Air exchange rate values [h^{-1}]

Figure A.14 shows the result of incorporating a wider range of air exchange rates when predicting α_{gw}. Here the central lines are the result corresponding to

$A_e = 0.5\,\mathrm{h}^{-1}$, while the upper and lower bounds of each shaded area correspond to $A_e = 0.1$ and $0.9\,\mathrm{h}^{-1}$ respectively. The shaded area cover much of the confidence interval of α_{gw} as a function of p_{in} This indicates that much of the uncertainty of numerically determining α_{gw} could be accounted for by considering the range of air exchange values at a site; a "numerical confidence interval" of sorts.

This concept of using pressure and air exchange rate is applied to a transient simulation, where we try to model a "typical" day by using the median diurnal variation of p_{in} and A_e are used as model inputs, where we consider our model with and without the preferential pathway present. Specifically, we will use the median diurnal values of p_{in} and A_e at one hour intervals over a 24-hour period from the ASU house and interpolating using cubic splines between these for continuity. This will be put into contrast for a case where we only use the median diurnal values of p_{in} but keep $A = 0.5\,\mathrm{h}^{-1}$ constant.

Figure A.15 shows how α_{gw} varies throughout this hypothetical "typical" day. Here we see that when the preferential pathway is present, variability of α_{gw} is mostly driven by fluctuations in contaminant entry rate; the variable and constant air exchange rate cases do not differ much from each other. When the preferential pathway is absent, then there is no variability of α_{gw} unless the air exchange rate is fluctuating.

To quantify the predicted variability of α_{gw} we define ratio between the minimum and maximum α_{gw} as

$$\Delta_{\max} = \frac{\alpha_{\mathrm{gw,max}}}{\alpha_{\mathrm{gw,min}}} \tag{A.13}$$

Applying this to the cases where air exchange rate is varied, and the preferential pathway present/absent we find that these ratios are $\Delta_{\max} = 5.09$ and $\Delta_{\max} = 1.68$ respectively. I.e. α_{gw} may be expected to vary around half an order of magnitude at site characterized by a preferential pathway under our considered conditions, whereas one where there is no preferential pathway may vary by a factor of 1.68.

These "maximum daily variability" $\Delta_{\max}$ values can be compared to those at the ASU house. Indoor contaminant concentration samples at the ASU house were collected roughly every four hours across the study period. By excluding the CPM period, and then resampling these data on a daily basis, we can find $\Delta_{\max}$ for each day. These data are further separated to consider the period before and after the land drain preferential pathway was closed. The period before the preferential pathway was closed then includes 441 days or data points, giving a median value $\Delta_{\max} = 2.33$. For the period after the preferential pathway was closed, we get 181 days of data, giving a median value of $\Delta_{\max} = 1.60$. Thus, we can see that we somewhat overpredicted the expected variability for the period when the preferential pathway was open, but quite close when it was closed.

This indicates that for sites that are characterized by diffusive transport, much of the observed variability of indoor contaminant concentrations are driven by fluctuations in air exchange rate. For sites dominated by advective transport, fluctuations in building pressurization, and subsequently contaminant entry, are more important drivers are temporal variability of α_{gw}.

A.4 Soil-Gas Spatial Variability & Preferential Pathways

Another aspect that preferential pathways has a significant impact on is spatial variability of contaminant vapors at a site. This can manifest inside the house itself, as large concentration differences between compartments, as was in the case of the leaky bathroom plumbing fixtures in the work by **pennell˙sewer˙2013**[**pennell˙sewer˙2013**]; here contaminant concentration were significantly higher in the upstairs bathroom than the basement, where higher concentrations are usually expected. These spatial variability can also manifest in the subsurface, which can be caused by a contaminant source[**chow˙concentration˙2007**], the building itself[**holton˙creation˙2018**], or as we will explore here - a subsurface preferential pathways.

A.4.1 ASU House

The influence of the ASU house land drain preferential pathway in causing a large spatial variation of contaminant vapors underneath the foundation slab, and in particular in the gravel sub-base layer, was explored and visualized in **guo˙identification˙2015**[**guo˙identif** work which can be seen in Figure A.16.

A.4.2 EPA Duplex

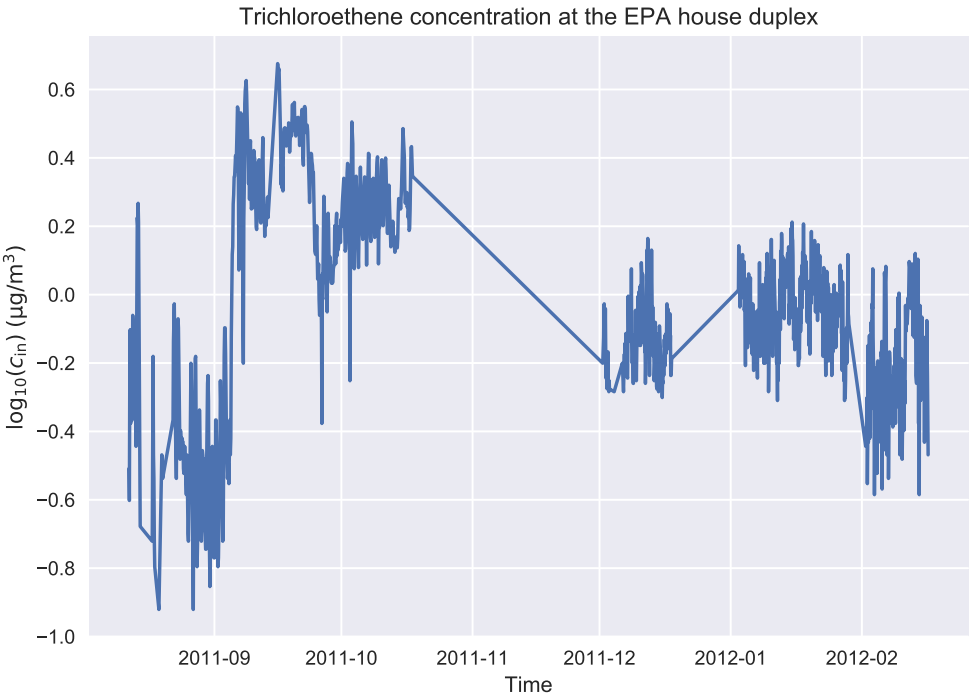

(a) Time series plot of the indoor TCE concentration in the heated side of the EPA duplex. Only the period before the SSD system was turned on considered.

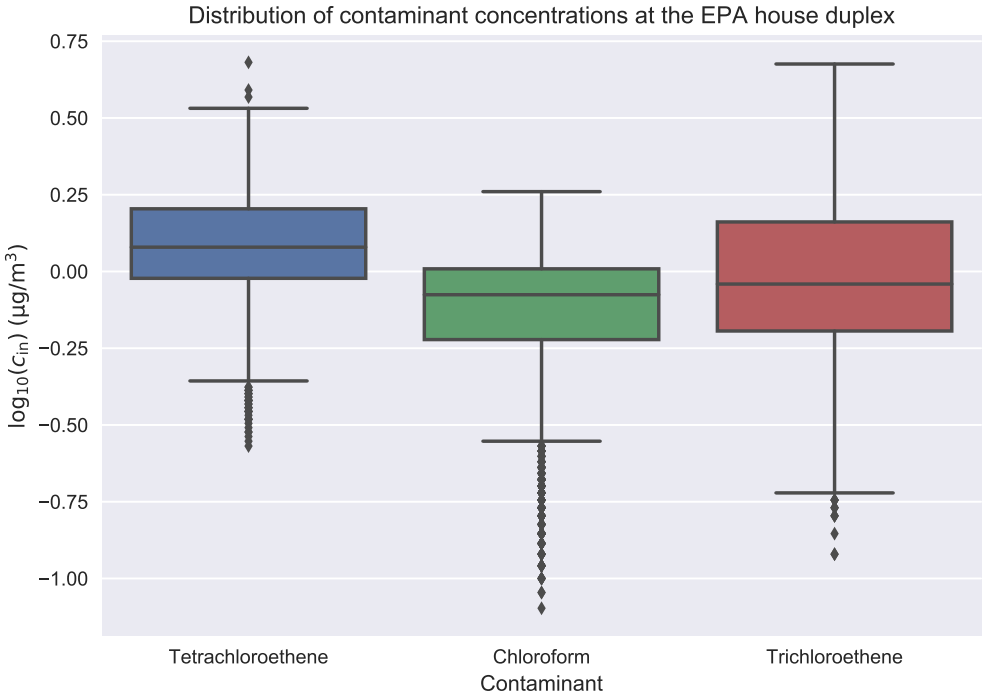

(b) Boxplot showing the distribution of log-10 transformed indoor concentration of three different contaminants in the heated side of the EPA duplex. The box is the interquartile range, with the line in the middle representing the median, and the top and bottom of the box representing the 75^{th} and 25^{th} percentiles respectively. The whiskers denote the extent of the data, with the points classified as "outliers", and are defined to be 1.5 times the IQR range.

Figure A.7: Time series of indoor TCE concentration over time at the EPA duplex and distribution of contaminant concentrations.

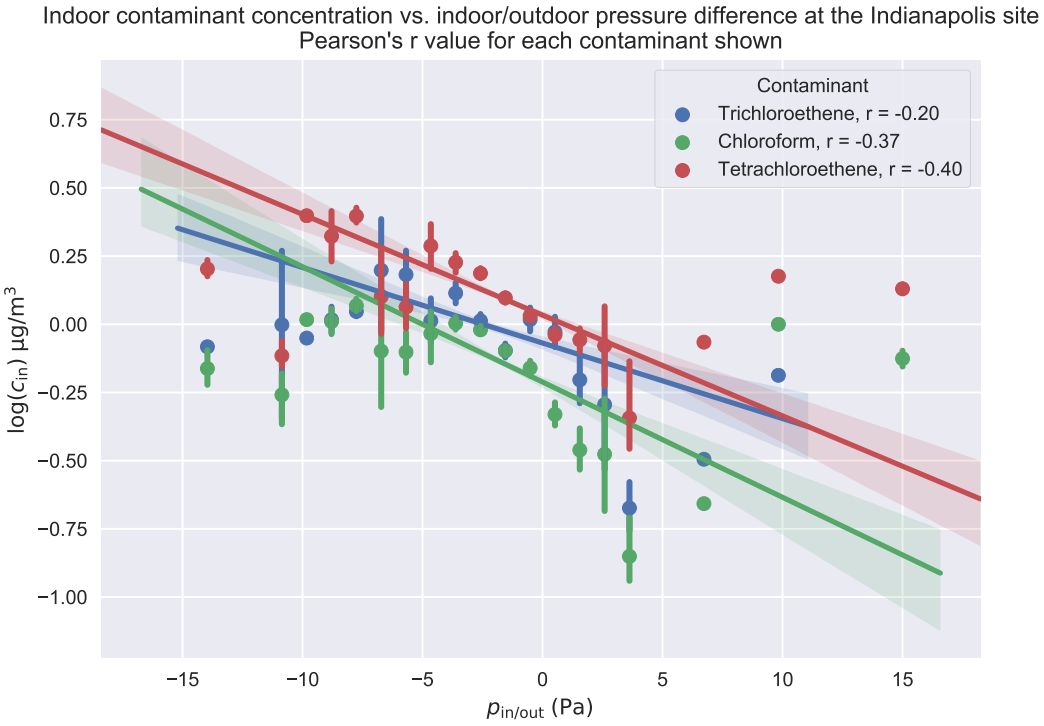

Figure A.8: Relationship between indoor/outdoor pressure difference and indoor contaminant concentration of three contaminants - TCE, PCE, and chloroform at the EPA duplex.

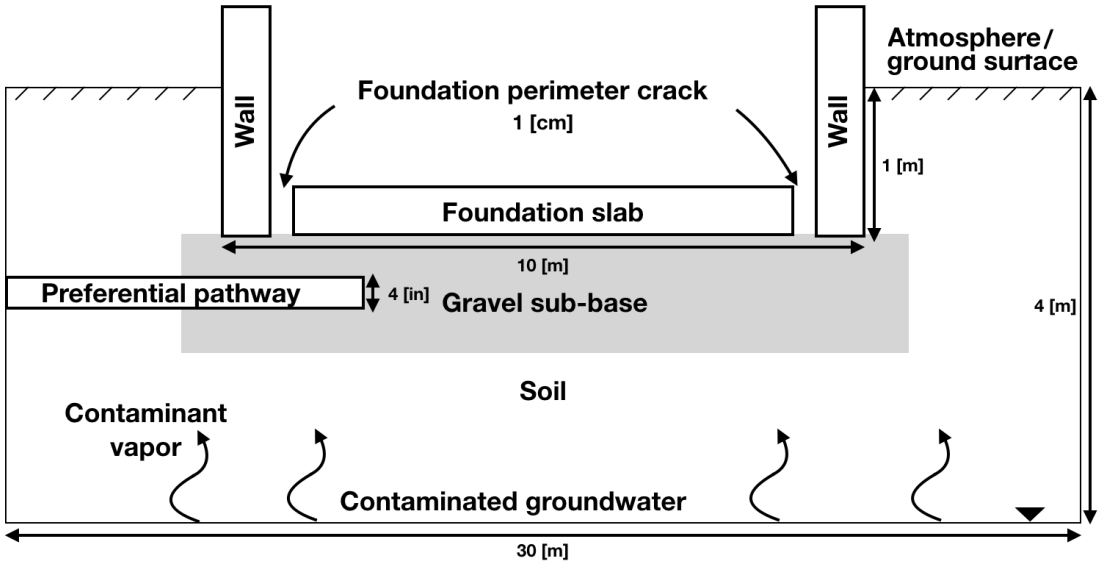

Figure A.9: The modeled preferential pathway VI scenario.

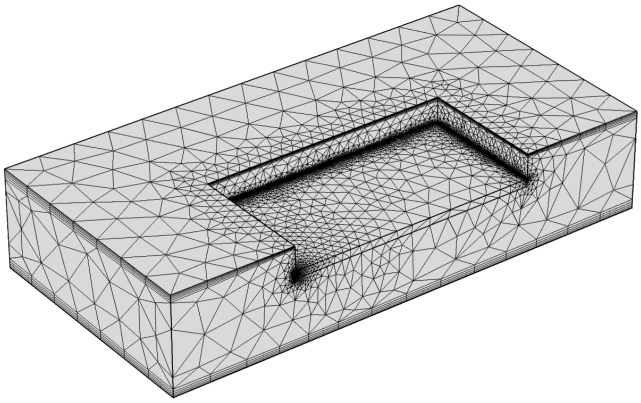

Figure A.10: Meshed geometry of the preferential pathway model. Notice the gravel sub-base layer and the preferential pathway exit.

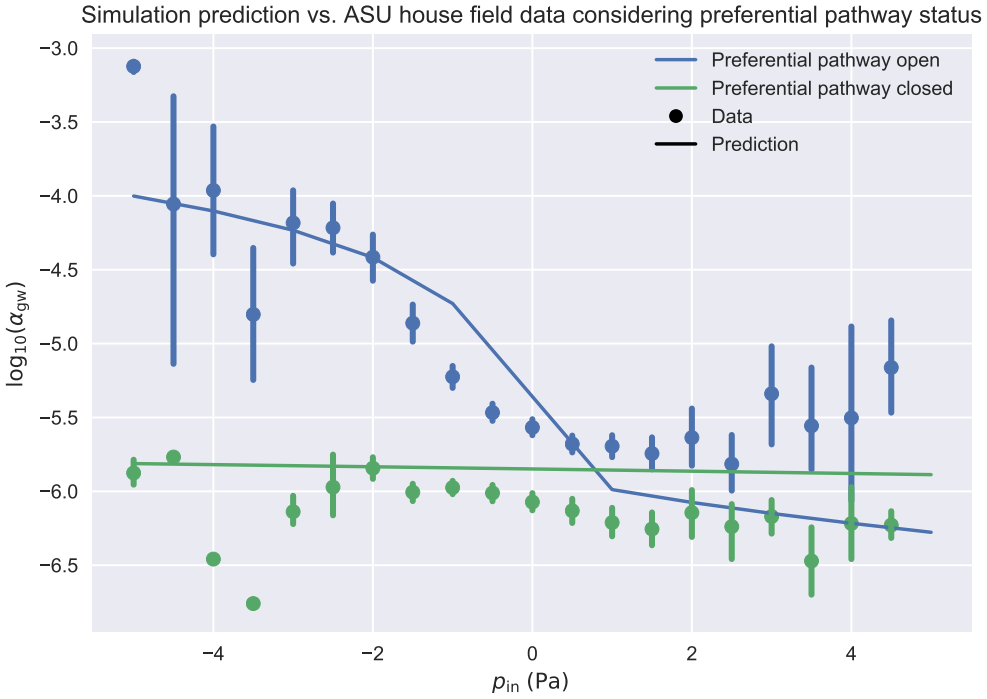

Figure A.11: Model predicted indoor air concentration (as groundwater attenuation) compared to values recorded at the ASU house. The modeling results are given the solid lines and data by the dots. Blue here represents data before the closing of the preferential pathway and modeling result from the corresponding model, i.e. the model features a preferential pathway and a gravel sub-base. The green color signifies data from the period after the closing of the preferential pathway with the corresponding model, i.e. the preferential pathway is removed but the gravel sub-base remains. Here the data is placed in 20 equally *spaced bin*, i.e. not equally *sized*. The dot is the mean value and the error bars represent the 95% confidence intervals.

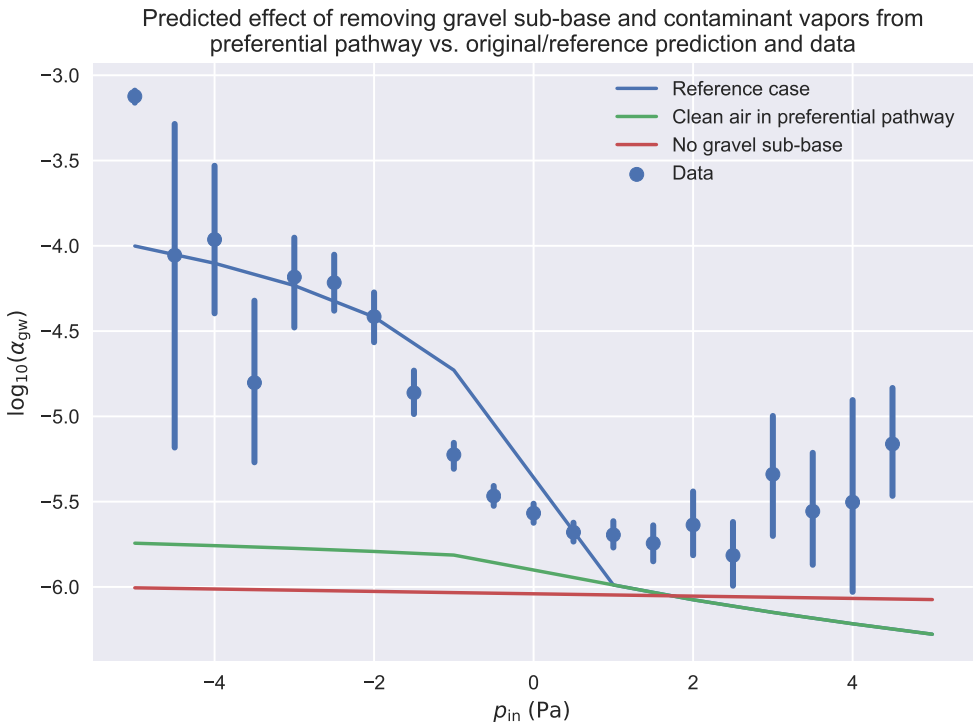

Figure A.12: How different cases affect the predicted impact of the preferential pathway. The effect of removing the gravel sub-base, as well as a clean-air containing preferential pathway are considered.

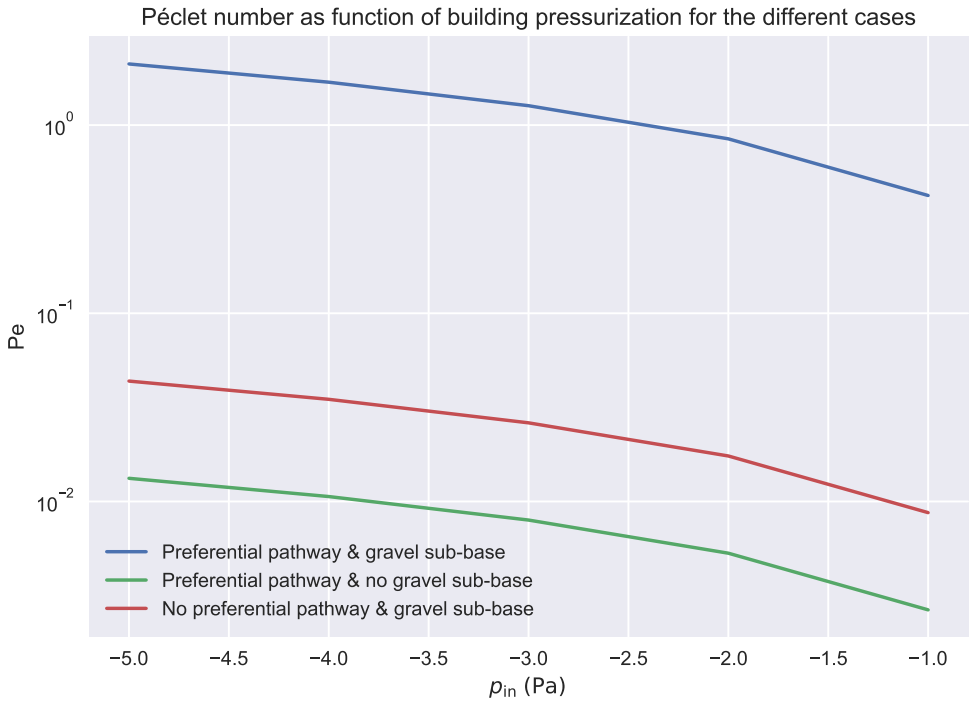

Figure A.13: Péclet number for transport through the foundation crack of our modeled house as a fucntion of building pressurization. Here we consider three cases where the preferential pathway and gravel sub-base are present/absent, which shows the dramatic effect these site features can have on contaminant transport at a VI site.

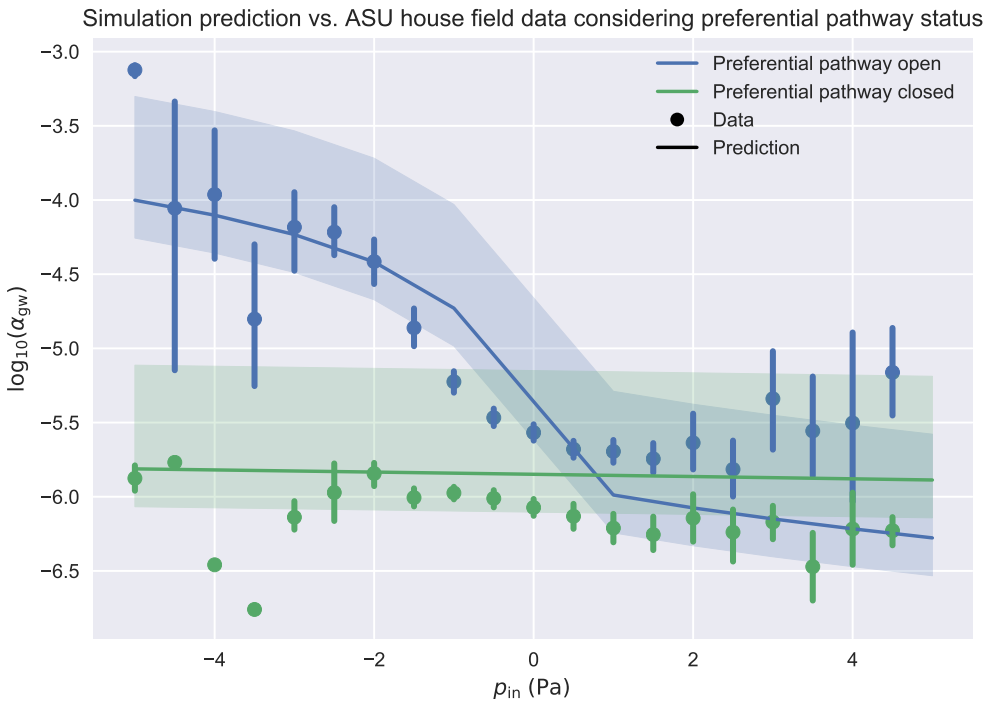

Figure A.14: Modeling result from Figure A.11 but with added shaded area to demonstrate the effect of different air exchange values. The central lines are the result corresponding to $A_e = 0.5\,\mathrm{h}^{-1}$, while the upper and lower bounds of each shaded area correspond to $A_e = 0.1$ and $0.9\,\mathrm{h}^{-1}$ respectively.

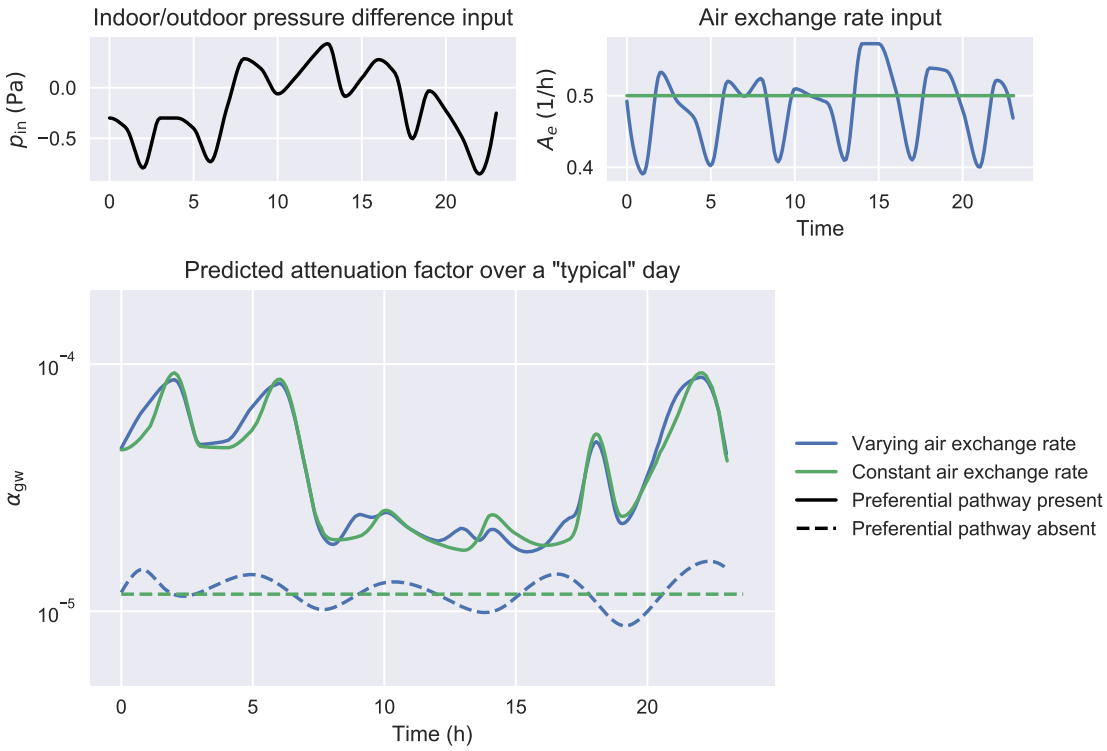

Figure A.15: Modeled indoor contaminant concentration (as attenuation from groundwater) over a "typical" day. Here the hourly median indoor/outdoor pressure difference and air exchange rates recorded at the ASU house, as well as a comparison case where a constant air exchange rate of $0.5\,\mathrm{h}^{-1}$ is assumed, are used as model input parameters. For these we consider two models cases; one where a preferential pathway is present and absent respectively.

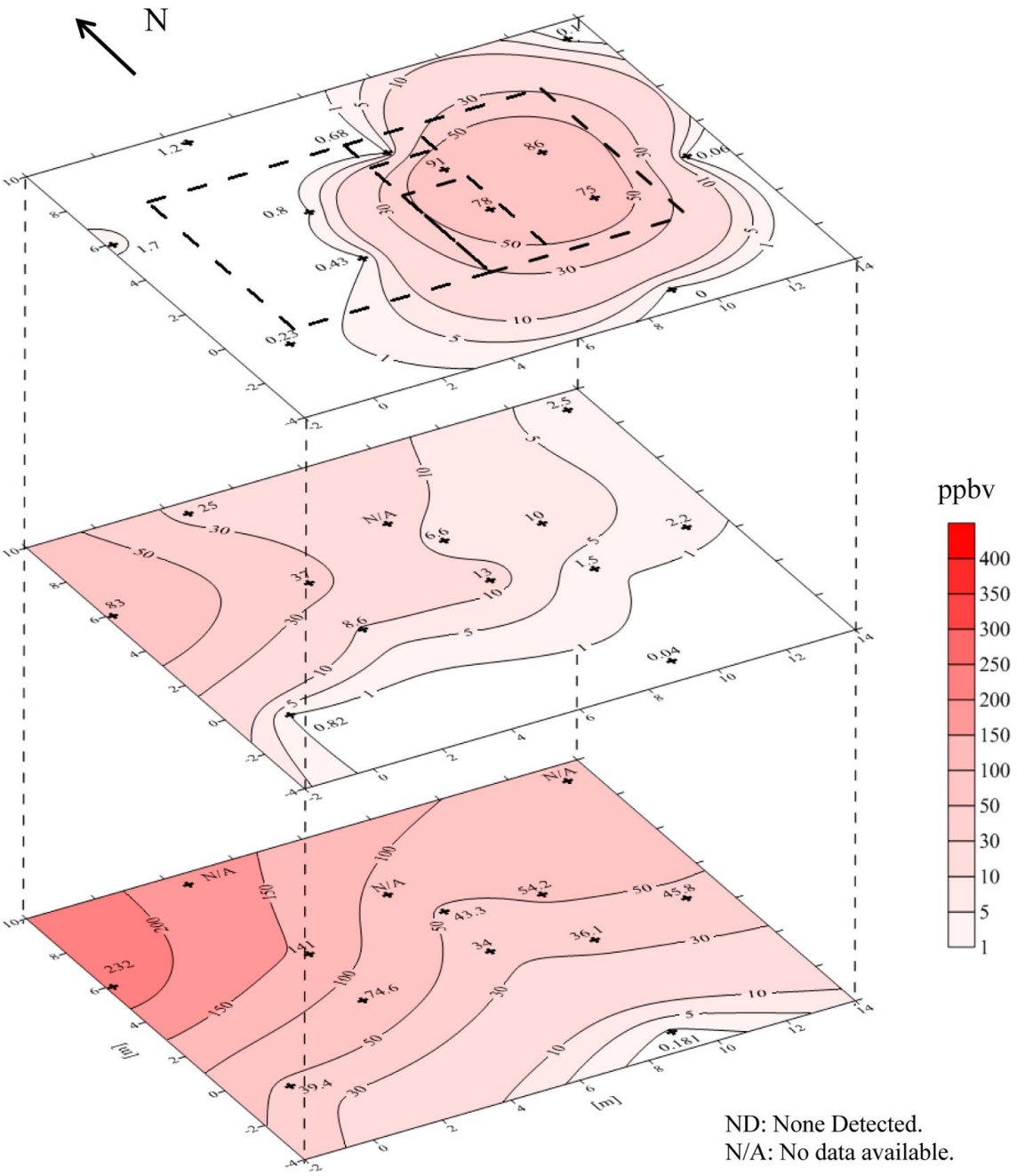

Figure A.16: Distribution of TCE contaminant vapors in the subsurface underneath the ASU house. The top layer is right beneath the foundation, with the two subsequent at 0.9 m and 1.8 m below the foundation slab.

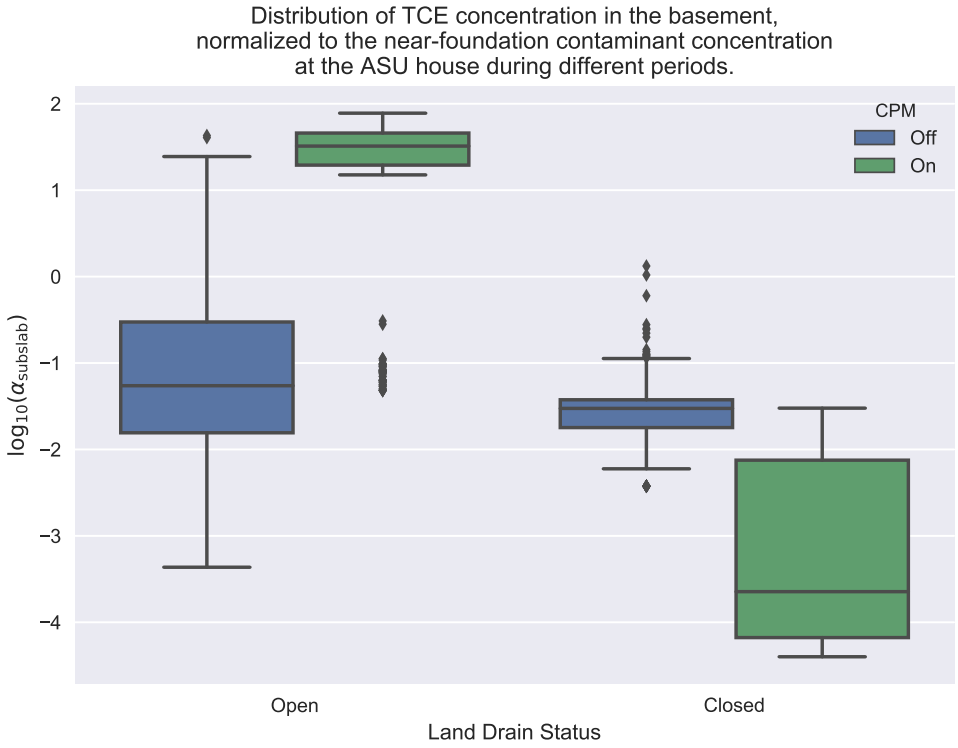

Figure A.17: TBD